Energy Reports 7 (2021) 6700–6717

Contents lists available at ScienceDirect

Energy Reports

journal homepage: www.elsevier.com/locate/egyr

Research paper

Variational mode decomposition based random forest model for solar radiation forecasting: New emerging machine learning technology

Mumtaz Ali [a], Ramendra Prasad [b], Yong Xiang [a], Mohsin Khan [c], Aitazaz Ahsan Farooque [d,e], Tianrui Zong [a], Zaher Mundher Yaseen [f,g,*]

[a] Deakin-SWU Joint Research Centre on Big Data, School of Information Technology, Deakin University, VIC 3125, Australia
[b] Department of Science, School of Science and Technology, The University of Fiji, Saweni, Lautoka, Fiji
[c] College of Mathematical Science Yangzhou University, Yangzhou 225002, China
[d] Faculty of Sustainable Design Engineering, University of Prince Edward Island, Charlottetown, PE C1A4P3, Canada
[e] School of Climate Change and Adaptation, University of of Prince Edward Island, Charlottetown, PE, Canada
[f] New Era and Development in Civil Engineering Research Group, Scientific Research Center, Al-Ayen University, Thi-Qar, 64001, Iraq
[g] College of Creative Design, Asia University, Taichung City, Taiwan

ARTICLE INFO

Article history:
Received 22 May 2021
Received in revised form 14 August 2021
Accepted 26 September 2021
Available online 18 October 2021

Keywords:
Solar radiation
Variational mode decomposition
Random forest
Simulated annealing
Volterra model
Energy

ABSTRACT

Forecasting of solar radiation (Radn) can provide an insight vision for the amount of green and friendly energy sources. Owing to the non-linearity and non-stationarity challenges caused by meteorological variables in forecasting Radn, a variational mode decomposition method is integrated with simulated annealing and random forest (VMD-SA-RF) for resolving this problem. Firstly, the input parameters are separated into training and testing phases after generating a one-day ahead significant lags at (t – 1). Secondly, the variational mode decomposition is set to factorize multivariate meteorological data of train and test sets, independently, into their band-limited signals. Thirdly, the simulate annealing based feature selection system is engaged to select the best band-limited signals. Finally, using the pertinent band-limited signals, the daily Radn is forecasted via random forest (RF) model. The outcomes are benchmarked with other comparative models. The hybrid fusion VMD-SA-RF model is tested geographically in Australia, generates reliable performance to forecast Radn. The hybrid VMD-SA-RF system combining the pertinent meteorological features, as the model predictors have substantial implications for renewable and sustainable energy resource management.

1. Introduction

With an upsurgeance of energy demand, there is an immense pressure on the utility suppliers to generate electricity from conventional coal and gas technologies (Hou et al., 2018). An alarming depletion rate of non-renewable energy generating sources and the subsequently increased concern about global warming issues have compelled the utility suppliers and the consumers to take up the challenge of incorporating environmentally friendly and renewable energy technologies into the utility grids (Hai et al., 2020). One such common technology is the roof-top solar photovoltaic (PV) systems connected via net-metring to the respective grids also referred as small-scale renewable energy schemes (SRES) and is common in the solar-rich Queensland state, Australia. Since 2016, Queensland has an unprecedented increase in renewable energy generations with 1706 MW of electricity generated from rooftop PV alone which is the highest level of rooftop PV systems in the country (Stock et al., 2017). Yet now the utility companies are facing a bigger challenge of providing a back-up whenever there is low or no energy production from grid-connected roof-top solar PV systems during overcast conditions and downtimes (Abbas and Azat, 2018). Additionally, the beginning of smart grid machinery with incorporation of recent electronic engineering has brought about connection of numerous complex instruments into the electrical networks whereby any large fluctuations from the normal power signal result in worst performances or lead to long-lasting costs in some scenarios (Mohmmoud, 2020; Soman et al., 2015). These issues are making the maintenance of power quality a serious concern and the analysts find SRES uneconomical (Chester et al., 2018). Unforeseen brownouts are proving to be costly for both the suppliers and the consumers and hence the rejection of such powerful renewable energy technology (Mohammed, 2018). Such in dispatchability, variability, and uncertainty of grid-connected SRES have presented unprecedented challenges to power grid operations and

* Corresponding author.
E-mail addresses: mumtaz.ali@deakin.edu.au (M. Ali), ramendrap23@gmail.com (R. Prasad), yong.xiang@deakin.edu.au (Y. Xiang), mohsinkhan7284@gmail.com (M. Khan), afarooque@upei.ca (A.A. Farooque), tianrui.zong@deakin.edu.au (T. Zong), zaheryaseen88@gmail.com (Z.M. Yaseen).

https://doi.org/10.1016/j.egyr.2021.09.113

planning (Sangrody et al., 2017). Hence, for apt planning, controlling and operations of smart utility grids integrated with solar PV systems, accurate Radn forecasting is imperative (Mahmmoud et al., 2020).

Since the machine learning (ML) algorithms are capable of 'learning' some of the entrenched features within the historical data in emulating future values Radn values, this could aptly be applied in smart grid technologies. Subsequently, Guermoui et al. (2018a) found that Gaussian process regression (GPR) methodology for Radn estimates provided the best results while in a study to forecast daily global and direct Radn using ML-based models, (Khelifi et al., 2020) found that multilayer perceptron and Radial Basis Function based neural network models perform well for three-step-ahead forecasting. A weighted Gaussian process regression (WGPR) was also developed and tested for daily global and direct horizontal Radn forecasting at multi-step forecast horizons (Guermoui et al., 2018b). The study revealed that WGPR Parallel Forecasting Architecture (WGPR-PFA) and WGPR Cascade Forecasting Architecture (WGPR-CFA) showed significant improvements in precision even at 10-steps ahead forecast horizon. Based on the reported database of Scopus for hybrid ML model for solar radiation forecasting, over 70 articles were appeared. Based on the generated VOSviewer algorithm, a substantial keywords presented for this research domain (Fig. 1a). In addition, based on the time scale of the adopted research (Fig. 1b), since 2016 and onward, the major researches were established and more research interest seen on the climate variability, development of new ML models such as deep learning model, and the insight on the energy harvesting. Fig. 1c states the major regions were investigated the solar radiation forecasting as it appears China region has the highest number of research; whereas, Australia region only four researches were adopted.

It is worth to mention, the stochastic nature of Radn due to the natural variability of solar irradiance compounded by environmental factors (such as cloud cover), atmospheric conditions (such as particulate matter and dust), latitude and season. Recently, a comprehensive literature review conducted by Guermoui et al. (2020), the research outlines the hybrid models developed for Radn forecasts and found that evidently single models may fail to find the desired solution and there is a need for more innovative hybridization methods. Hence, to increase the forecast precision of ML modelling approaches, data pre-processing via multi-resolution analysis (MRA) needs to be incorporated. Fourier spectra are one of the earliest approaches for frequency investigation of a static signal, yet the method essentially fails with biases which are non-static such as those in Radn time series (Soman et al., 2015). Then came Fourier transformations, which only accomplishes transformation of frequency resolutions without the time stamp (Prasad et al., 2019). While, in predicting scenarios, the discrete wavelet transformation (DWT) has promisingly accepted however, the basic flaw of DWT is the intrinsic devastation influence that restrains the features and produces only half the wavelet coefficients, and by high and low pass filters (Rathinasamy et al., 2014), the remaining flat version is again and again treated at a rough resolution. With that the performance of DWT largely depends upon the option of mother wavelet and the number of putrefaction levels which is selected *a priori* (Soman et al., 2015). DWT has also poor adaptability to signals. To ameliorate these issues, a data-dependent demarcation technique is more suited in comparison to the conventional wavelet techniques, which is known as Empirical Mode Decomposition (EMD) founded by Huang et al. (1998). The EMD lacks appropriate mathematical reasoning behind its structure. The variants of EMD together with, Ensemble based EMD (Wu and Huang, 2009), complete ensemble EMD with adaptive noise (CEEMDAN) (Torres et al., 2011) and improved complete ensemble empirical mode decomposition with adaptive noise (ICEEMDAN) (Ali and Prasad, 2019), have been gradually established to handle the drawback of their respective predecessors. The EMD and its variants have been preferred due to their self-adaptability making it completely data-dependent in extracting salient predictive information without loss of underpinning features (Alvanitopoulos et al., 2014; Prasad et al., 2018). Further, the EMD based decomposition preserves the physical configurations of the sequential predictors (Wu et al., 2011).

Despite such progressive evolution of the remarkable MRA tool, the EMD based decomposition techniques can only be implemented to decompose a single input attribute at a time (Ali et al., 2019; Ali and Prasad, 2019). For instance, only the important historical lags of daily Radn could be utilized to predict the prospective Radn values, which a major issue with EMD, since as aforementioned, Radn is contingent upon a number of key predictors. In such a multiple inputs case, a sequential decomposition needs to be adopted following (Prasad et al., 2019), which though is a promising approach, yet, in sequential decomposition approach, some pertinent information may not be lucid since each EMD demarcation is carried out in isolation. To overcome this challenge and incorporate multiple predictor inputs with simultaneous decomposition an advanced and versatile version of EMD *viz.*, variational mode decomposition (VMD) is being designed to resolve the entrenched sub-frequency components of respective inputs.

The VMD is able to extract the entrenched predictive information concurrently from multiple non-stationary and non-linear historic data series via an appropriate multi-resolution analysing approach. As a result, only the most significant set of predictors need to be screened out as irrelevant ones that may obscure the model. Moreover, another important benefit of the VMD is its adaptive and non-recursive nature which is entirely dependent on the predictor variables and thus needing trivial human effort during decomposition process (Dragomiretskiy and Zosso, 2014). Unlike the EMD technique (Looney and Mandic, 2009), the VMD demarcates and updated the input predictors into various band-limited intrinsic mode functions (BL-IMFs) overcoming the mode mixing difficulty and misclassification problem produced by fixed algorithm in EMD (Li et al., 2017). The VMD is fundamentally more robust in terms of sampling and noise reduction together with astound accuracy in embedded frequency search and separation. Moreover, the VMD algorithm is able to aptly extract the time–frequency signals via band limiting and optimization (Dragomiretskiy and Zosso, 2014). These salient features ascertain the suitability of VMD as a multichannel MRA utility, yet the application of the algorithm in the short-term such as daily Radn forecasting has not been piloted up to now. The VMD-based ML algorithms have been utilized in bearing fault detection (Li et al., 2017); air quality parameter estimation (Wang et al., 2017) together with wind power prediction (Zhang et al., 2018) and wind modelling (Zhou et al., 2018). Recently, Majumder et al. (2018) forecasted solar irradiance (kWh/m^2) using VMD in combination with reduced Morlet Wavelet Kernel extreme learning machine. However, the length of the data used was very short i.e., 1 year only, which would essentially mean that the ML model did not get sufficient proficiency in capturing the embedded trends and data features as many of these features may have not been introduced to the model due to very short training data set.

This paper develops a novel hybrid model that addresses non-stationarity issues in multiple predictor inputs using self-adaptive approach whilst generating accurate forecasts of short-term, i.e., daily Radn, using over 110 years of solar radiation data in order to provide adequate and pertinent information to the ML models. The novelty and contribution include:

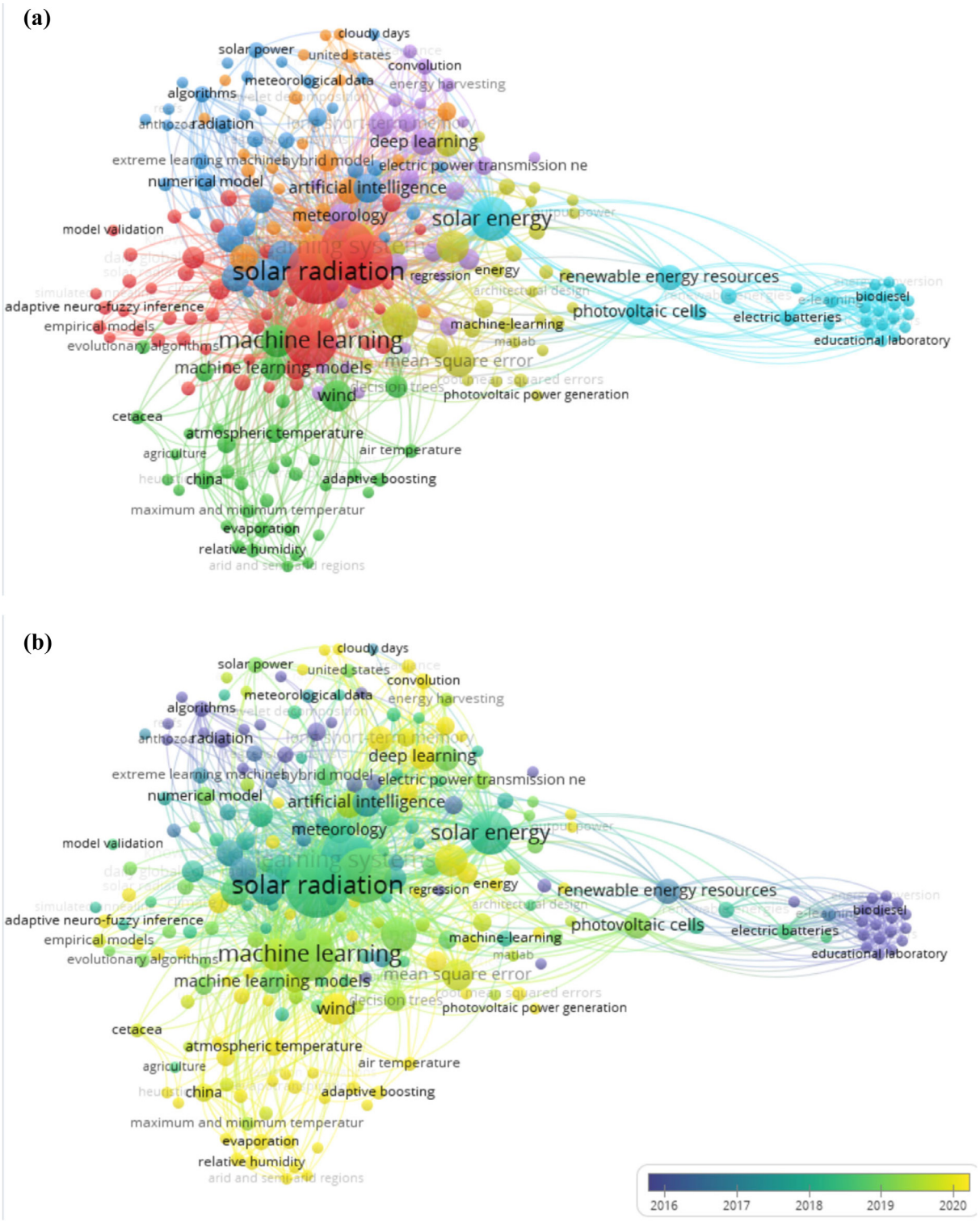

Fig. 1. (a) The major keywords reported over the literature for solar radiation using hybrid ML models, (b) time line of the adopted keywords over the literature, (c) number of conducted researches over the literature.

i. Utilizing the variational mode decomposition (VMD) method, being a non-iterative data decomposition procedure. During VMD process, concurrent demarcation and extraction of BL-IMFs are carried out, making it advantageous over EMD and its variants which are recursive and computationally inefficient.

ii. The simulated annealing (SA) is a bio-inspired adaptive and non-deterministic feature selection method ideal for feature optimizations. The SA algorithm approach is implemented to rank and decide the best BL-IMFs in training phase to build the model.

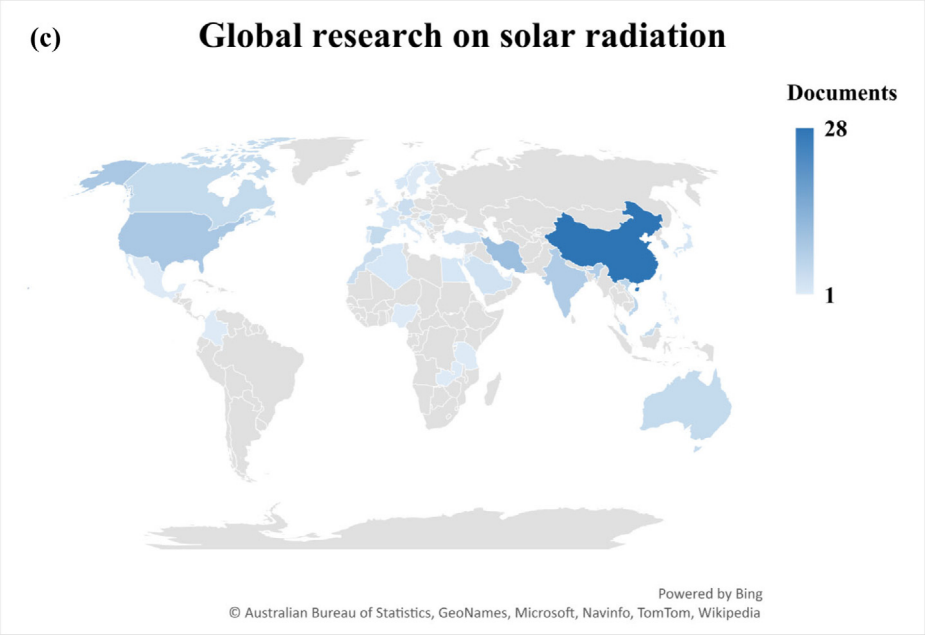

Fig. 1. (*continued*).

iii. The RF model is then applied to establish the VMD-SA-RF model to forecast the daily Radn based on the selected BL-IMFs.

An evaluation of the predicting efficiency of the novel VMD-SA-RF model is performed with similar VMD-SA integrations of Multivariate adaptive regression splines (MARS), (i.e., VMD-SA-MARS), Volterra (i.e., VMD-SA-Volterra) and the standalone RF, MARS and Volterra models. The hybrid VMD-SA-RF with benchmark models was developed and evaluated at three sites within sunshine-state, Queensland, Australia. The next section of the paper presents the theoretical framework of ML techniques, followed by this is Section 3 Case Study Description and Data Used. Then Section 4 presents the Results, Section 5 is Discussion with Further Analysis with Section 6 with Concluding Remarks.

2. Theoretical framework of machine learning techniques

The theoretical frameworks of variational mode decomposition (VMD), Simulated annealing (SA) feature optimization algorithm, the forecasting RF model and its comparative counterpart Multivariate Auto Regressive Spline (MARS) and Volterra models are presented in this section.

2.1. Method of variational mode decomposition (VMD)

The VMD algorithm developed by Dragomiretskiy and Zosso (2014), which is to ameliorate the disadvantages of recursive EMD algorithm (Looney and Mandic, 2009). During the VMD, the predictor variable is decomposed into several band limited sub-signals (BL-IMFs), which essentially are amplitude-modulated-frequency modulated (Dragomiretskiy and Zosso, 2014). Sparsity natures of BL-IMFs are revealed when reproducing the input signal. In mathematical terms, the *i*th mode can be written as:

$$M_i = A_i(t)\cos(\vartheta_i(t)) \tag{1}$$

where $A_i(t)$ = instantaneous amplitude, and $\vartheta_i(t)$ = instantaneous phase. While the derivative of $\vartheta_i(t)$ is the instantaneous frequency.

The algorithm constructs an analytical signal for each mode M_i via Hilbert transformation and computes the unilateral frequency spectrum. Consequently, employing the displacement property of the Fourier transformation, the spectrum of the sub-signals is altered to baseband and the first order H^1 Gaussian smoothness is employed to estimate the bandwidth. The minimization of the total spectral bandwidths of the entire IMFs range is the key aim of VMD algorithm. Since the sum of the modes is equivalent to the actual undecomposed variable, it induces a significant constraint, however, with the implementation of Lagrangian multiplier together with a quadratic penalty term the issue is resolved. Finally, the Alternating Direction Method of Multipliers is working to iteratively demarcate the undecomposed signals via VMD into the respective BL-IMF components. For full details of the algorithm, readers can refer to (Dragomiretskiy and Zosso, 2014).

2.2. Simulated annealing (SA) algorithm

The SA algorithm is an attribute selection based on biological strategies to discover an appropriate solution for an optimization problem (Elleithy and Fattah, 2012). Fundamentally, the SA is a non-deterministic characterized based optimization system that can be describe as following:

(a) Generate a suitable random solution in the initial phase.
(b) Using cost function to estimate the cost in above (a).
(c) Again, estimate random neighbouring solution.
(d) The cost can be calculated for above solution in (c).
(e) The $\cos t(a) > \cos t(b)$, generate a new solution otherwise step (f).
(f) Repeat (c)–(e) until an ideal solution is discovered.

The implementation of SA algorithm in real world problems are includes: travelling salesman (Peng et al., 1996), computer-simulated holograms (Taniguchi et al., 1997), power productivity (Wilson, 1997) and heat transfers (Athier et al., 1997).

2.3. Random Forest (RF) model

Bootstrapping and bagging is the underpinning technique on which the RF ensemble modelling approach is constructed upon,

for accurate prediction in the form of decision trees (Breiman, 2001, 1996). Using a random bagging technique, the RF algorithm model is a regression tree based ML method which develops groups (Al-Sulttani et al., 2021). By selecting well-known predictors every node is connected in a random way to proceed robust performance while avoiding overfitting (Bhagat et al., 2020). The RF is constructed in the following stages:

i. Using bootstrapping to generate n-number of trees (i.e., n_{trees}) by embedding the inputs.
ii. With a non-prune regression tree using a chaotic sample of inputs ($m$try), pick the maximum number of split predictors.
iii. To forecast Rdn in terms of aggregations, combine the estimates of n_{trees}.

The applications of RF model have evidenced its capacity in diverse climate, environment and hydrology domains (Ali et al., 2020; Bhagat et al., 2020; Sharafati et al., 2019; Tiyasha et al., 2021).

2.4. Model of Multivariate Auto Regressive Spline (MARS)

MARS model was firstly introduced by Friedman (1991), the MARS model essentially partitions the dataset into several splines that are of equal lengths. The data are further split into numerous subgroups at respective knots, whereby the relationships of the predictor and the target variable are described by two of a kind basis functions (BF) producing consistent simulations with continuous spin-offs (Friedman, 1991). Mathematically at location ρ, the output (O) of the ith subclass of the knot can be found as:

$$\left.\begin{array}{l} O = \mathrm{BF}_i(x) = \max(0, x-\rho) \\ \quad \textit{and its mirror}: \\ O = \mathrm{BF}_i(x) = \max(0, k-\rho) \end{array}\right\} \tag{2}$$

Finally, the outputs of the series of *BF*s are summed that generates a large and potentially bulky model that generally overfit the training data. Hence, those *BF*s that make least contributions towards the performance of the model, calculated on the basis of minimum Generalized Cross Validation (GCV) are pruned in a backwards-deletion strategy. This results in a much smaller and less bulky optimal model.

2.5. Volterra model

The Volterra model based on Taylor series mathematical extension to emulate non-linear systems with causal dependence. A 2nd-order representation has been utilized following earlier studies (Labat et al., 2001; Maheswaran and Khosa, 2012b,a; Rathinasamy et al., 2014). For the 2nd-order Volterra algorithm, the output $[y(t)]$ whereby the Volterra kernels are $v_1(\beta_1)$ and $v_2(\beta_1, \beta_2)$ can mathematically be expressed as:

$$y(t) = V_{k1}[x(t)] + V_{k2}[x(t)] \tag{3}$$

A further shortening of the above equation (Eq. (3)) gives:

$$y(t) = V_{k1}[x(t)] + V_{k2}[x(t)] \tag{4}$$

where $V_{k1}[x(t)]$ = 1st order Volterra operator and $V_{k2}[x(t)]$ = 2nd order Volterra operator.

A multiple input single output (MISO) system emerges when many input time series as used as inputs, as is the case with the current forecasting of daily Radn. The 2nd order Volterra series for MISO case is:

$$\begin{aligned} y(t) = & \sum_{\alpha=1}^{A}\sum_{\beta=1}^{B} v_1^{(\beta)}(\alpha)\, x_\beta(t-\alpha) \\ & + \sum_{\beta=1}^{B}\sum_{\gamma=1}^{A}\sum_{\alpha=1}^{A} v_{2s}^{(\beta)}(\gamma,\alpha)\, x_\beta(t-\gamma)\, x_\beta(t-\alpha) \\ & + \sum_{\beta 1}^{B}\sum_{\beta 2=1}^{\beta 1-1}\sum_{i=1}^{A}\sum_{\alpha=1}^{A} v_{2\times}^{(\beta 1,\beta 2)}(\gamma,\alpha)\, x_{\beta 1}(t-\gamma)\, x_{\beta 2}(t-\alpha) \end{aligned} \tag{5}$$

where the number of predictor inputs is represented by B, and A represents the length of memory of each selected input. The $v_1^{(\beta)}$ = 1st order kernel self kernel, $v_{2s}^{(\beta)}$ = 2nd order self kernel and $v_{2\times}^{(\beta 1,\beta 2)}$ = second 2nd order cross-kernel. An orthogonal least squares method was adopted in the estimation of Volterra kernels.

3. Case study description and data used

3.1. Data collection and preparation

To develop a robust model, a large set of predictor variables consisting of meteorological variables were collated that included Potential Evapotranspiration (FAO56), evaporation (Evap), vapour pressure (VP), Relative Humidity at maximum and minimum temperature ($\mathrm{RH_{max}}$.T, $\mathrm{RH_{min}}$.T), monthly precipitation (Rain), maximum and minimum temperature ($T_{\max,}\mathrm{T_{min}}$) as illustrated in Table 1a. While the daily mean Radn data series were used as the target from January 1905 to June 2018 in developing the models. Three sites situated in Queensland, i.e., Site 1: Ipswich, Site 2: Goldcoast, and Site 3: Darling Downs were selected (Table 1b). The Scientific Information for Land Owners (SILO) provided the predictor and target data sets (Jeffrey et al., 2001). Robust statistical techniques were utilized to interpolate the missing data points (Beesley et al., 2009; Zajaczkowski et al., 2013).

The descriptive statistics (Table 1) reveals the stochastic nature of daily Radn data and the respective predictor inputs. The skewness of the predictors and the daily Radn data ranged between −1 and 1, showing symmetrical distributions, except for $\mathrm{RH_{min}}$.T which illustrated negative skewness (skewness ≤ -2.4) at all three sites. A near to normal distributions with $-1 \leq$ kurtosis ≤ -1.0 was also evident for the data sets at all three sites, excepting for the distribution of $\mathrm{RH_{min}}$.T that had longer positive tails at all sites.

3.2. Study locations

The Australian continent receives a high level of solar radiation annually making Australia very conducive for electricity generation through solar radiation (Zahedi, 2010). The study sites are located in Queensland State, known as the sunshine state of Australia, that receives a profusion of Radn with fewer overcast days and the state government is committed to increase the energy generation by renewables to up to 50% by the year 2030 (Stock et al., 2017). Fig. 2 illustrates a diagram showing the geographical positions of the regions while Table 1 summarizes the longitude, latitude, combined with differing elevations. The sites were ideally selected due to their relevance to renewable energy generations. The Darling Downs site has a 110 MW large-scale solar generation solar PV project being committed, while Ipswich is a booming city, a high growth in the quantity of grid-connected rooftop solar PV systems have been noted with installation of the largest shopping mall based solar array having a generation capacity of 30 kWh was recently commissioned. Additionally, Gold Coast site has very high electricity demand,

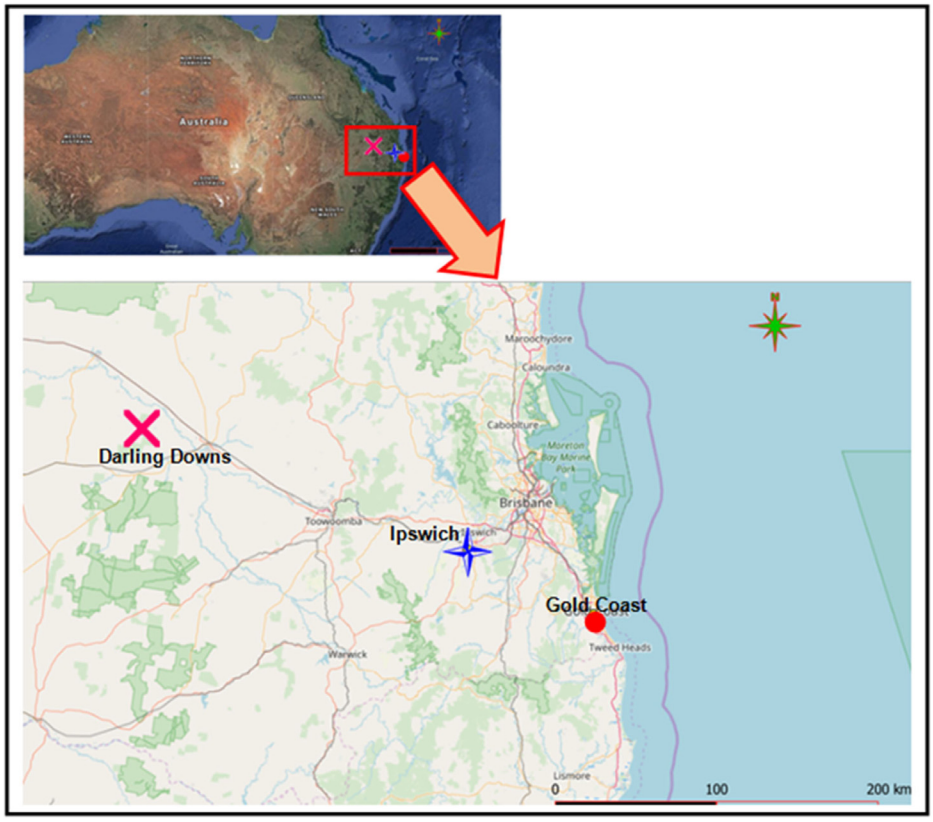

Fig. 2. Map of Australia showing the study sites for daily solar radiation forecasting.

Table 1
Basic statistics of the meteorological predictors and target variable in addition with geographic coordinates of the locations.

Sites	**Ipswich**					**Gold coast**					**Darling Downs**				
Long. (°E)	**153.68**					**153.40**					**150.88**				
Lat. (°N)	**27.695**					**28.01**					**27.11**				
Elevation (m)	**50**					**13.1**					**353**				
Meteorological predictors	**Mean**	**Max**	**Min**	**Std.**	**Skew**	**Mean**	**Max**	**Min**	**Std.**	**Skew**	**Mean**	**Max**	**Min**	**Std.**	**Skew**
$T._{Max}$	24.3	41.5	12	3.4	0.1	25.0	42.0	10.5	3.7	0.0	26.2	44.0	7.5	5.8	−0.1
$T._{Min}$	17.4	27.5	2.5	4.1	−0.4	15.3	26.0	−0.5	4.6	−0.4	11.7	28.0	−6.0	6.3	−0.4
Evap	4.2	21.6	0.2	1.5	0.3	4.2	21.2	0.2	1.5	0.4	5.3	16.8	0.2	2.2	0.2
VP	18.7	38.0	2.0	5.3	−0.1	17.8	37.0	2.0	5.3	0.0	14.7	30.0	1.0	4.9	0.1
$RH_{Max}.T$	60.2	100	7.3	12.1	−0.2	54.9	100.0	6.9	11.8	0.1	42.3	100	4.0	11.5	0.7
$RH_{Min}.T$	89.6	100	10	11.0	−1.4	94.1	100.0	12.5	9.5	−2.3	94.4	100	13.2	9.6	−2.4
FAO56	3.6	8.6	0.6	1.2	0.3	3.6	8.9	0.5	1.3	0.3	4.1	8.9	0.5	1.7	0.2
Rain	18.6	35.0	0.0	6.0	−0.1	18.6	35.0	2.0	6.0	−0.1	19.4	33.0	4.0	5.9	−0.2

yet no large scale solar generation facility has been proposed for this city. The nearest solar farm is situated at Sunshine Coast and it would be interesting to perform studies and verify the Radn forecasts for Gold Coast to assist the decisionmakers in planning future renewable energy facilities.

3.3. The forecasting accuracy tools

To predict Radn via some statistical metrics, the performance of VMD-SA-RF *vs*. VMD-SA-MARS, VMD-SA-Volterra, single-phase RF, single-phase MARS and single-phase Volterra models were studied. These metrics are denoted by the following mathematical equations (Tiyasha and Yaseen, 2020; Tur and Yontem, 2021; Yaseen, 2021):

I. Coefficient of Correlation (R):

$$R = \left(\frac{\sum_{i=1}^{N} \left(Radn^{Obs,i} - \overline{Radn^{Obs,i}} \right) \left(Radn^{For,i} - \overline{Radn^{For,i}} \right)}{\sqrt{\sum_{i=1}^{N} \left(Radn^{Obs,i} - \overline{Radn^{Obs,i}} \right)^2} \sqrt{\sum_{i=1}^{N} \left(Radn^{For,i} - \overline{Radn^{For,i}} \right)^2}} \right) \tag{6}$$

II. The mathematical form of Willmott's Index (E_{WI}) is as follows:

$$E_{WI} = 1 - \left[\frac{\sum_{i=1}^{N} \left(Radn^{For,i} - Radn^{Obs,i} \right)^2}{\sum_{i=1}^{N} \left(\left| Radn^{For,i} - \overline{Radn^{Obs,i}} \right| + \left| Radn^{Obs,i} - \overline{Radn^{Obs,i}} \right| \right)^2} \right], \quad 0 \le E_{WI} \le 1 \tag{7}$$

III. Nash–Sutcliffe efficiency (E_{NS}) value:

$$E_{NS} = 1 - \left[\frac{\sum_{i=1}^{N} \left(Radn^{Obs,i} - Radn^{For,i}\right)^2}{\sum_{i=1}^{N} \left(\overline{Radn^{Obs,i}} - \overline{Radn^{For,i}}\right)^2} \right], 0 \le E_{NS} \le 1 \quad (8)$$

IV. The Mathematical derivation of Root mean square error ($RMSE$) is as:

$$RMSE = \sqrt{\frac{1}{N} \sum_{i=1}^{N} \left(Radn^{For,i} - Radn^{Obs,i}\right)^2} \quad (9)$$

V. Mean absolute error (MAE):

$$MAE = \frac{1}{N} \sum_{i=1}^{N} \left| \left(Radn^{For,i} - Radn^{Obs,i}\right) \right| \quad (10)$$

VI. Legates and McCabe's (E_{LM}):

$$E_{LM} = 1 - \left[\frac{\sum_{i=1}^{N} \left| Radn^{For,i} - Radn^{Obs,i} \right|}{\sum_{i=1}^{N} \left| Radn^{Obs,i} - \overline{Radn^{Obs,i}} \right|} \right], 0 \le E_{LM} \le 1 \quad (11)$$

VII. Relative root mean squared percentage error ($RRMSPE$; %), is expressed as

$$RRMSPE = \frac{1}{N} \sum_{i=1}^{N} \left| \frac{\left(Radn^{For,i} - Radn^{Obs,i}\right)}{Radn^{Obs,i}} \right| \times 100 \quad (12)$$

VIII. Relative mean absolute percentage error ($RMAPE$; %):

$$RMAPE = \frac{1}{N} \sum_{i=1}^{N} \left| \frac{\left(Radn^{For,i} - Radn^{Obs,i}\right)}{Radn^{Obs,i}} \right| \times 100 \quad (13)$$

In Eqs. (6)–(13), $Radn^{Obs,i}$, $Radn^{For,i}$ are the observed and forecasted ith magnitudes of solar radiation, while $\overline{Radn^{Obs,i}}$ and $\overline{Radn^{For,i}}$ denote the observed and forecasted mean $Radn$ values separately, where N is the entire value of testing data records.

3.4. Designing of the VMD-SA-RF model

The VMD-SA-RF approach is established in MATLAB R2018b programming (The Math Works Inc. USA). Specification of the PC (2.93 GHz dual-core Pentium 4 operating system), through which the whole simulation results were attained. The dataset is divided into 70% (train) and 30% (test) before designing the model. Since a multiresolution analysis toom (VMD) was adopted in this study, only one antecedent time lagged inputs (i.e., $t - 1$) of $T._{Max}$; $T._{Min}$; Evap; VP; RH_{Max}.T; RH_{Min}.T; and FAO56 were used in the model development to forecast daily Radn as elucidated in the following phases.

Phase 1 VMD process

The training input predictors are demarcated by applying the VMD method into precise BL-IMFs and residuals. Furthermore, the predefined parameters contain moderate bandwidth constraint ($\alpha = 2000$), noise-tolerance ($\tau = 0$), modes/IMFs (k), omega initialization ($init = 0$) and tolerance of convergence condition ($tol = 0$). To obtain the equal number of BL-IMFs for testing, the VMD method is conditioned with modes (see Table 2). Total 49 VMD signals with residuals (Table 2) for all three sites (i.e., Darling Downs, Ipswich, Gold Coast) is draw out with each input has (BL-IMFs = 7).

Phase 2: The SA Scheme

The SA methodology is implemented to indicate the best and suitable BL-IMFs in training subset for model construction. The predefined further, some constraints/parameters comprises maximum no. of iterations (=10) and initial temperature (=10). The amount of designated most BL-IMFs is decided to 15 features that were consider earlier to execute the SA technique (see; Table 3). For testing phase equal number of BL-IMFs were picked based on selected BL-IMFs training session. The advantages of SA algorithm is that it may not only prevent the population from falling into a local optimal solution, but also increase the diversity of the population. Further, the optimization will be unstable due to the randomness (Du et al., 2018). Moreover, SA can deal with arbitrary systems and cost functions and statistically guarantees to find an optimal solution. In fact, it has been proved that SA will converge to its global optimality (Yang, 2020). For more detail on SA, we refer to the readers (Dowsland and Thompson, 2012; Kirkpatrick et al., 1983; Yang, 2020).

Phase 3: Normalization procedure

With the help of Eq. (13) (Salih et al., 2019), to handle large fluctuation and spikes in the data (Hsu et al., 2003), the training and testing sets are modified between [0, 1].

$$\sigma_{Norm} = \frac{(\sigma - \sigma_{Min}())}{(\sigma Min_{Max})} \quad (14)$$

where σ symbolizes the data point, σ_{Min} = the least data record, σ_{Max} = the largest data point and σ_{Norm} = the desired normalized point.

Phase 4: Applying RF model

The last modelling phase is based on employing the RF algorithm to predict daily Radn to study its capability over a near-real timescale. After incorporating the BL-IMFs lags into the RF algorithm, several kinds of parameters were used to tune the model that includes 1000 trees and 5 predictors. To test the forecasting accuracy of the fused VMD-SA-RF approach, the identical BL-IMFs signals were chosen from test set following the train set. To compare the results, the MARS and Volterra models are also combine with the VMD and SA to build VMD-SA-MARS and VMD-SA-Volterra models. Further, the single-phase RF, MARS and Volterra methods were also compared (Table 4). Fig. 3 explains the graphic representation of the VMD-SA-RF system.

The RMSE, MAE and R assessment tools were implemented to measure the VMD-SA-RF precision during training stage against VMD-SA-MARS, VMD-SA-Volterra, single-phase RF, single-phase MARS and single-phase Volterra models.

VMD-SA-RF model generates the quantities of RMSE, MAE and R, for Radn predicting at Ipswich are seen to be: RMSE = 1.47 MJm^{-2}, MAE = 1.06 MJm^{-2}, R = 0.974. For comparison models, these matrices are: VMD-SA-MARS [RMSE = 3.62 MJm^{-2}; MAE = 2.66 MJm^{-2}, R = 0.783], VMD-SA-Volterra [RMSE = 3.62 MJm^{-2}; MAE = 2.67 MJm^{-2}; R = 0.782], single-phase RF [RMSE = 2.14 MJm^{-2}; MAE = 1.54 MJm^{-2}; R = 0.937], single-phase MARS [RMSE = 3.71 MJm^{-2}; MAE = 2.64 MJm^{-2}; R = 0.769] and single-phase Volterra single-phase RF [RMSE = 3.72 MJm^{-2}; MAE = 2.65 MJm^{-2}; R = 0.769].

Similarly, the proposed VMD-SA-RF approach realistically achieves better forecasts for Gold Coast and Darling Downs in comparison with benchmarking models (see; Table 4). Therefore, it is apparent that the VMD-SA-RF will be accurate for testing scenarios to Radn at all three sites.

4. Applications results and analysis

To forecast Radn in Queensland, Australia, for highly three rich solar radiation, locations were initiated the VMD-SA-RF model. The forecasting accuracy of VMD-SA-RF is estimated with respect to VMD-SA-MARS, VMD-SA-Volterra, single-phase RF,

Table 2
Design parameters involved in decomposing mode signals for training and testing period in each study site using VMD method.

	Training period				Testing period			
	Moderate bandwidth constraint α	Noise-tolerance τ	No. of modes κ in each input	No. of total modes signals	Moderate bandwidth constraint α	Noise-tolerance τ	No. of modes κ in each input	No. of total modes signals
Ipswich	2000	0	7	49	2000	0	7	49
Gold Coast	2000	0	7	49	2000	0	7	49
Darling Downs	2000	0	7	49	2000	0	7	49

Table 3
Number of selected VMD signals using the SA algorithm, training, and testing data points. Note that the VMDs were selected at $(t-1)$ lag.

Sites	No. of selected modes signals	Max. iteration	Initial temperature	No. of data points in each station	No. of training data	No. of testing data
Ipswich	15	10	10	47411	3200	14211
Gold Coast	15	10	10	47411	3200	14211
Darling Downs	15	10	10	47411	3200	14211

Table 4
Training performance of VMD-SA-RF vs. VMD-SA-MARS, VMD-SA-Volterra, single-phase RF, single-phase MARS and single-phase Volterra models with correlation coefficient - *R*, *RMSE* and *MAE* (MJm^{-2}).

	VMD-SA-RF			**VMD-SA-MARS**			**VMD-SA-Volterra**		
	Training period			**Training period**			**Training period**		
	RMSE **(MJm^{-2})**	***MAE*** **(MJm^{-2})**	***R***	***RMSE*** **(MJm^{-2})**	***MAE*** **(MJm^{-2})**	***R***	***RMSE*** **(MJm^{-2})**	***MAE*** **(MJm^{-2})**	***R***
Ipswich	1.47	1.06	0.974	3.62	2.66	0.783	3.62	2.67	0.782
Gold Coast	1.39	0.99	0.976	3.40	2.51	0.810	2.53	3.42	0.808
Darling Downs	1.324	0.944	0.978	3.22	2.44	0.829	3.22	2.43	0.829
	Single-phase RF			**Single-phase MARS**			**Single-phase Volterra**		
	Training period			**Training period**			**Training period**		
	RMSE **(MJm^{-2})**	***MAE*** **(MJm^{-2})**	***R***	***RMSE*** **(MJm^{-2})**	***MAE*** **(MJm^{-2})**	***R***	***RMSE*** **(MJm^{-2})**	***MAE*** **(MJm^{-2})**	***R***
Ipswich	2.14	1.54	0.937	3.71	2.64	0.769	3.72	2.65	0.769
Gold Coast	2.16	1.55	0.934	3.67	2.61	0.774	0.773	3.68	2.62
Darling Downs	1.92	1.37	0.946	3.33	2.42	0.817	0.814	3.34	2.44

Table 5
Testing performance of VMD-SA-RF vs. VMD-SA-MARS, VMD-SA-Volterra, single-phase RF, single-phase MARS and single-phase Volterra models measured by *R*, *RMSE*, and *MAE* (MJm^{-2}).

Site 1: Ipswich			
	R	*RMSE* (MJm^{-2})	*MAE* (MJm^{-2})
Single-phase MARS	0.684	4.69	3.58
Single-phase Volterra	0.694	4.69	3.54
Single-phase RF	0.933	2.47	1.83
VMD-SA-MARS	0.739	4.48	3.16
VMD-SA-Volterra	0.735	4.44	3.21
VMD-SA-RF	**0.972**	**1.72**	**1.28**
Site 2: Gold Coast			
Single-phase MARS	0.738	4.36	3.29
Single-phase Volterra	0.739	4.37	3.26
Single-phase RF	0.945	2.24	1.66
VMD-SA-MARS	0.763	4.20	3.25
VMD-SA-Volterra	0.765	4.13	3.10
VMD-SA-RF	**0.974**	**1.66**	**1.22**
Site 3: Darling Downs			
Single-phase MARS	0.690	4.73	3.33
Single-phase Volterra	0.696	4.76	3.28
Single-phase RF	0.934	2.46	1.82
VMD-SA-MARS	0.709	4.74	3.80
VMD-SA-Volterra	0.715	4.48	3.50
VMD-SA-RF	**0.971**	**1.81**	**1.37**

single-phase MARS and single-phase Volterra models based on *R*, *RMSE* and *MAE* errors.

The VMD-SA-RF model established for Ipswich region accomplish the maximum amounts of R and lowermost RMSE and MAE magnitudes in forecasting Radn (R ≈ 0.972, RMSE ≈ 1.72 MJm^{-2}, MAE ≈ 1.28 MJm^{-2}) in comparison with VMD-SA-MARS (R ≈ 0.739, RMSE ≈ 4.48 MJm^{-2}, MAE ≈ 3.16 MJm^{-2}), VMD-SA-Volterra (R ≈ 0.735, RMSE ≈ 4.44 MJm^{-2}, MAE ≈ 3.21 MJm^{-2}), single-phase RF (R ≈ 0.933, RMSE ≈ 2.47 MJm^{-2}, MAE ≈ 1.83 MJm^{-2}), single-phase MARS (R ≈ 0.684, RMSE ≈ 4.69 MJm^{-2}, MAE ≈ 3.58 MJm^{-2}) and single-phase Volterra (R ≈ 0.694, RMSE ≈ 4.69 MJm^{-2}, MAE ≈ 3.54 MJm^{-2}). Equally, the VMD-SA-RF

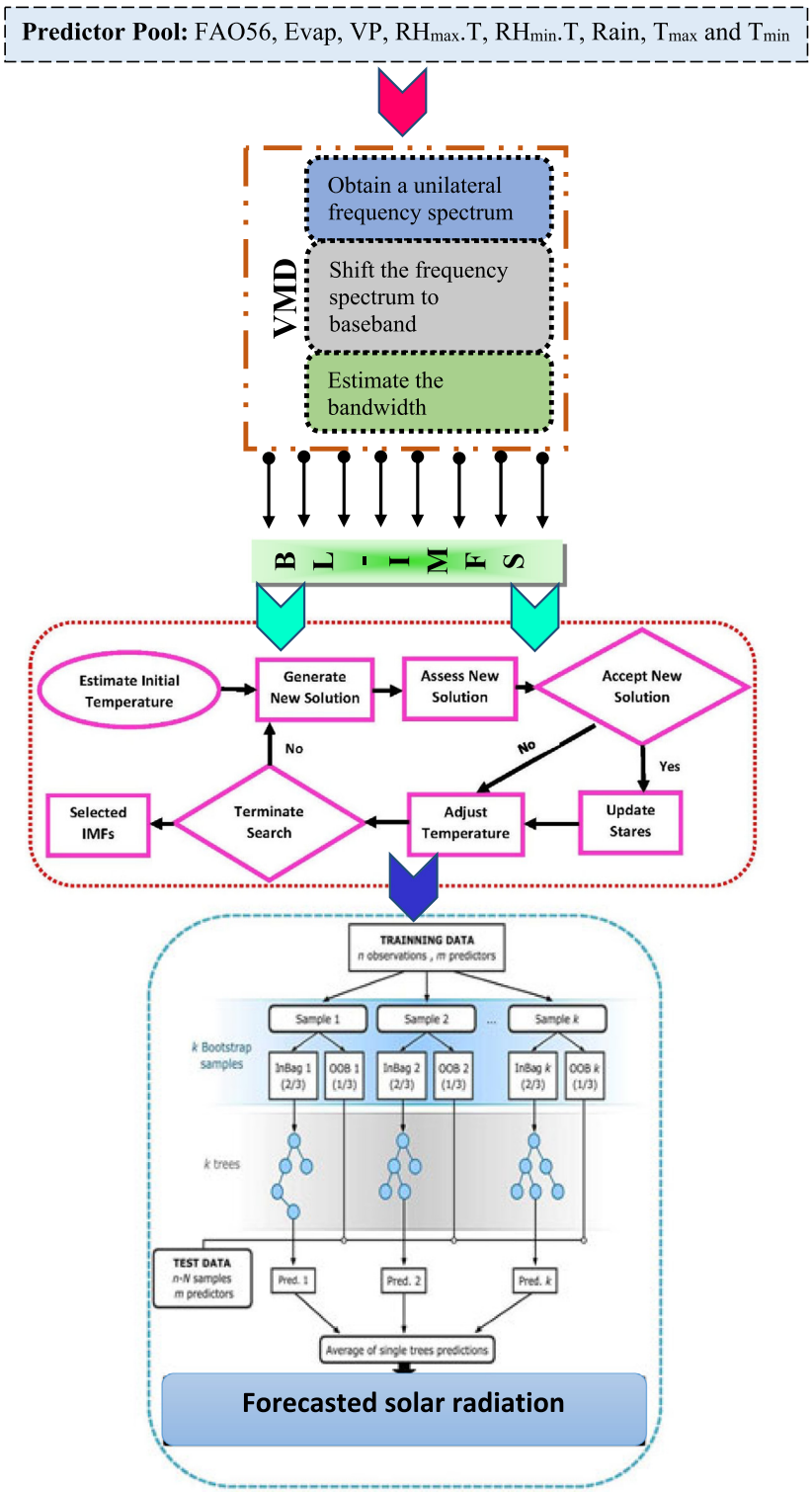

Fig. 3. Schematic diagram of VMD-SA-RF model used to forecast daily solar radiation.

generates considerably healthier forecasts for the Gold Coast and Darling Downs (Table 5) regions. This establishes that VMD-SA-RF can be implemented a well-designed forecasting tool for Radn forecast in contrast to VMD-SA-MARS, VMD-SA-Volterra, single-phase RF, single-phase MARS and single-phase Volterra.

Table 6 uses other useful multiple criteria based on E_{WI}, E_{NS} and E_{LM} to examine the VMD-SA-RF vs. VMD-SA-MARS, VMD-SA-Volterra, single-phase RF, single-phase MARS and single-phase Volterra models. According to these measures, the results produced by VMD-SA-RF for Ipswich are ($E_{WI} \approx 0.957$, $E_{NS} \approx 0.926$ and $E_{LM} \approx 0.758$), followed by single-phase RF ($E_{WI} \approx 0.904$, $E_{NS} \approx 0.847$ and $E_{LM} \approx 0.653$), VMD-SA-MARS ($E_{WI} \approx 0.759$, $E_{NS} \approx 0.499$ and $E_{LM} \approx 0.403$), VMD-SA-MARS ($E_{WI} \approx 0.753$, $E_{NS} \approx 0.509$ and $E_{LM} \approx 0.394$), single-phase Volterra ($E_{WI} \approx 0.640$, $E_{NS} \approx 0.451$ and $E_{LM} \approx 0.331$) and single-phase MARS ($E_{WI} \approx 0.609$, $E_{NS} \approx 0.451$ and $E_{LM} \approx 0.323$) models.

Table 6
The performance of VMD-SA-RF vs. VMD-SA-MARS, VMD-SA-Volterra, single-phase RF, single-phase MARS and single-phase Volterra models using Willmott's index (E_{WI}), Nash–Sutcliffe(E_{NS}) and Legates-McCabe's (E_{LM}) agreement. Note that the best model is boldfaced (**blue**).

Site 1: Ipswich			
Models	E_{WI}	E_{NS}	E_{LM}
Single-phase MARS	0.609	0.451	0.323
Single-phase Volterra	0.640	0.451	0.331
Single-phase RF	0.904	0.847	0.653
VMD-SA-MARS	0.759	0.499	0.403
VMD-SA-Volterra	0.753	0.509	0.394
VMD-SA-RF	**0.957**	**0.926**	**0.758**
Site 2: Gold Coast			
Single-phase MARS	0.722	0.535	0.383
Single-phase Volterra	0.733	0.533	0.387
Single-phase RF	0.927	0.877	0.689
VMD-SA-MARS	0.711	0.569	0.391
VMD-SA-Volterra	0.741	0.584	0.418
VMD-SA-RF	**0.962**	**0.933**	**0.771**
Site 3: Darling Downs			
Single-phase MARS	0.707	0.444	0.371
Single-phase Volterra	0.733	0.435	0.380
Single-phase RF	0.905	0.849	0.656
VMD-SA-MARS	0.620	0.439	0.283
VMD-SA-Volterra	0.693	0.501	0.339
VMD-SA-RF	**0.951**	**0.918**	**0.741**

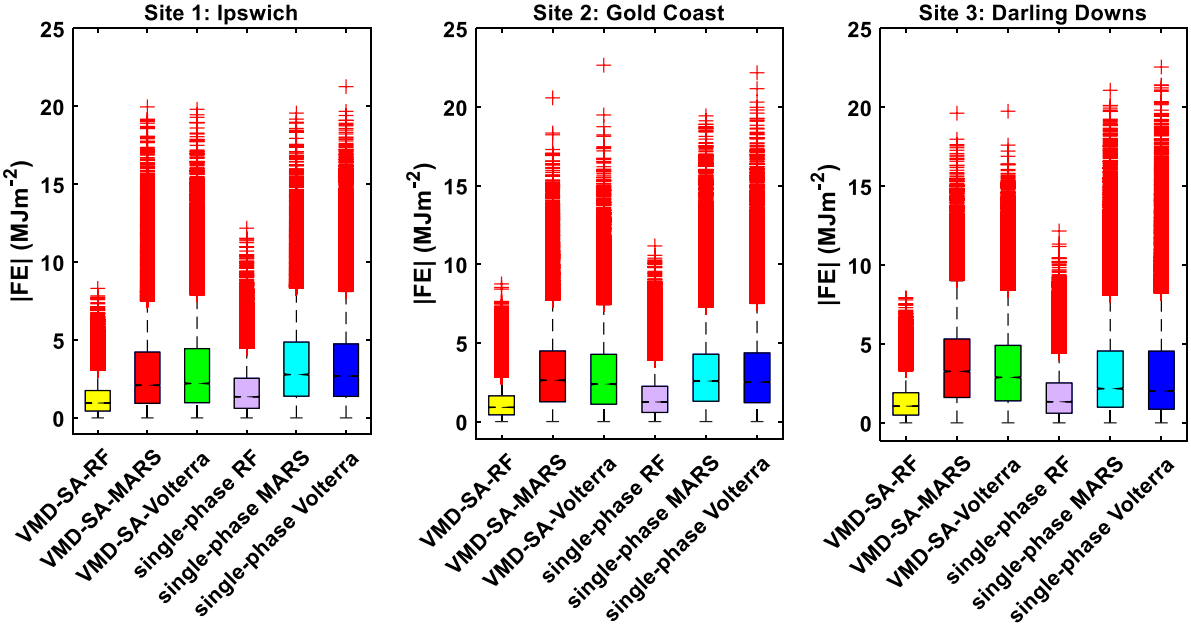

Fig. 4. Boxplots showing the actual error generated between the forecasted and observed Radn by the VMD-SA-RF vs. the VMD-SA-MARS, VMD-SA-Volterra, single-phase RF, single-phase MARS and single-phase Volterra models in the testing phase.

For Gold Coast and Darling Downs sites, again the VMD-SA-RF acts as a good model exhibiting ($E_{WI} \approx 0.962$, $E_{NS} \approx 0.933$ and $E_{LM} \approx 0.771$) and ($E_{WI} \approx 0.951$, $E_{NS} \approx 0.918$ and $E_{LM} \approx 0.741$) respectively. The scores attained by benchmarking models (Table 6) backing the supremacy of the VMD-SA-RF. When applied for Radn forecasting all sites could be pointed as 'very satisfactory' at these three sites in Australia for the projected hybrid VMD-SA-RF model according to the said criteria. Its highly recommended that models with ENS < 0.800 are 'unsatisfactory', those between $[0.800, 0.900]$ are 'fairly good' and ENS > 0.900 is conceived to be 'very satisfactory' (Shamseldin, 1997).

Furthermore, diagnostic plots were commenced using the model assessment. Preceding to making the box-plots, during the testing period forecasting errors ($|FE|$) were calculated. When $|FE|$ ideally plotted on box plots this need to be zero, for best performing models the disposition of FE requires to be near to zero as possible. For ease of understanding the absolute FE ($|FE|$) quantities were mapped. Showing its better forecasting capability, Fig. 4 displays the VMD-SA-RF model at all sites documented smaller $|FE|$ divisions in agreement with Tables 4 and 5. To that of the VMD-SA-RF model, the single-phase RF model looked to have a very immediate performance of relative models followed by the normalized metrics, E_{WI}, E_{NS}, and E_{LM}. On the contrary, since for all three sites (Ipswich, Gold Coast and Darling Downs) the distribution generated from the VMD-SA-RF model were equally spread with a huge number of outliers points the box-plots make a clear distinction of performances. Additionally, in Fig. 5 plots were also plotted to get a transparent image of the forecast

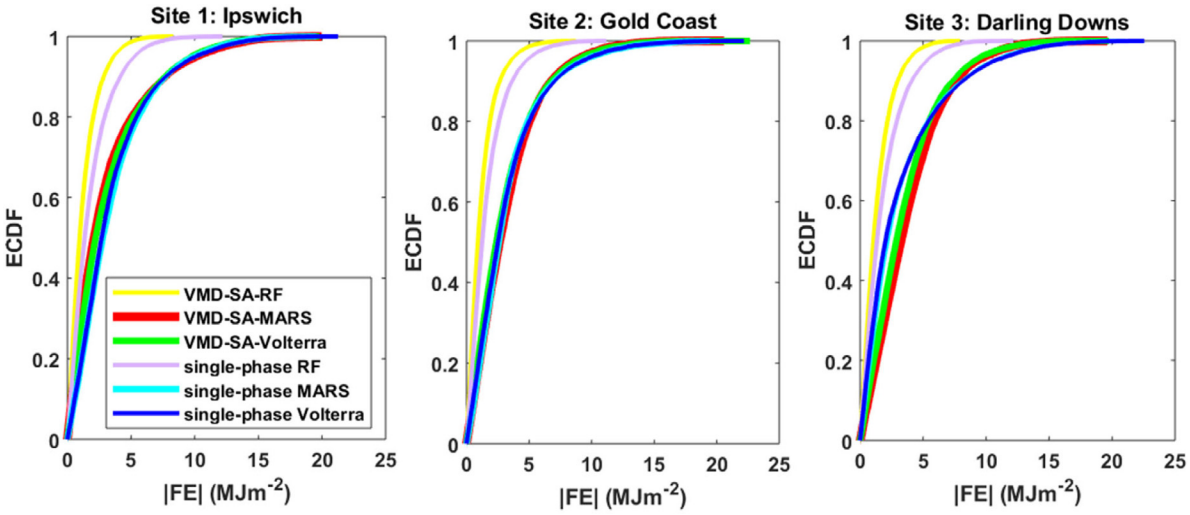

Fig. 5. ECDF of the forecasting error (FE) generated by the VMD-SA-RF vs. the VMD-SA-MARS, VMD-SA-Volterra, single-phase RF, single-phase MARS and single-phase Volterra models applied at the three tested study sites.

error distributions the empirical cumulative distribution function (ECDF). For all three sites, the ECDF line plots of VMD-SA-MARS, VMD-SA-Volterra, single-phase RF single-phase MARS and single-phase Volterra displayed a very close profile. A notable narrow profile restricted within the least range was displayed the ECDF profile of VMD-SA-RF at all three sites on the other hand. Therefore, for all three sites, the box-plots (Fig. 4) collectively with the ECDF plots (Fig. 5) further determines the greater performance of the VMD-SA-RF model in forecasting daily Radn analysed to the disputing models.

To assess holistically the efficiency of model, the quantity of correlation *R* is mapped in the shape of the Taylor diagram that allows an extra thorough evaluation of the model performances. Concerning standard deviations, the Taylor diagram (Fig. 6) reveals an extra tactile and conclusive reference statistically between the forecasted and observed Radn relying on *R*. It is demonstrated that the single-phase MARS and Volterra with their hybrid models are not relevant as the *R* to standard deviation points were highly divided from the exemplary mentioned point. In this study, the planned hybrid VMD-SA-RF model was lying close to the mentioned Radn which maintains the forecasting accuracy was pointedly higher at all 3-sites than the other 3-associating models.

Based on R, the performance of bar graph plots (Fig. 7) was further diagnosed. Note that, by the corresponding models (VMD-SA-RF, VMD-SA-MARS, VMD-SA-Volterra, single-phase RF, single-phase MARS and single-phase Volterra), the curiosity here is to assess all models that can be successfully emulated. Entering lower R values the single-phase MARS and Volterra models at all sites execute not very good. Obviously, in contrast with the competing models the VMD-SA-RF model possess greater R values at all 3-sites. Subsequently, over 95% of forecasts can be ideally generated by this model. Explicitly, results indicated that for the case of Ipswich (R $\approx$ 0.972), Gold Coast (*R* $\approx$ 0.974) and Darling Downs (R $\approx$ 0.971), which coincide with the conclusion in Tables 5 and 6.

At three remarkable positions a difference in performances of models is apparent after the conclusions of the numerical metrics (Tables 5 and 6). To differentiate models at dimensionally different positions their inability is the key limitation of these metrics. The comparative performance (Table 7) properly revealed that the VMD-SA-RF model show the lowermost values of RRMSPE and RMAPE in contrast through VMD-SA-MARS, VMD-SA-Volterra, single-phase RF, single-phase MARS and single-phase Volterra models for all three sites. More precisely, the RRMSPE and RMAPE extents when relating VMD-SA-RF through the 2nd best acting model single-phase RF, in the aggregation [VMD-SA-RF: single-phase RF] were as follows: Ipswich: [9.35%, 9.68%: 13.46%, 13.84%]; Gold Coast: [8.61%, 8.61%: 13.84%, 12.13%] and Darling Downs: [9.86%, 10.42%: 13.40%, 13.87%]. Consequently, the RRMSPE and RMAPE revealed that the VMD-SA-RF established the best accuracy for Site 2-Gold Coast, and after that Site 1-Ipswich and Site 3- Darling Downs.

To display precise interpretations on the predicting capacity of the designed systems, Fig. 8 exhibits a comprehensive clarification by plotting the frequency distribution of |FE| errors generated by VMD-SA-RF *vs.* benchmarking models. The attained |FE| errors of the VMD-SA-RF were inside the lowest range of ($\pm$15) for all three sites. Fig. 8 portrays the general assessment of VMD-SA-RF was healthier in this research.

A stem plot showing the RRMSPE produced by the VMD-SA-RF *vs.* the VMD-SA-MARS, VMD-SA-Volterra, single-phase RF, single-phase MARS and single-phase Volterra models is shown in Fig. 9 for the three sites under study. Based on the outcomes of the percentage RRMSPE error magnitudes, which are considerably lower for the VMD-SA-RF model in comparison to other models, the VMD-SA-RF outperforms at all sites. Most notably, the error for the VMD-SA-RF model is less than 10% for all three sites, confirming a high-performance model.

Fig. 10 displays a scatterplot in terms of r^2 between forecasted and actual Radn. The VMD-SA-RF is undoubtedly better than benchmark counterparts in terms of r^2 (VMD-SA-RF $\approx$ 0.945, VMD-SA-MARS $\approx$ 0.547, VMD-SA-Volterra $\approx$ 0.540, single-phase RF $\approx$ 0.871, single-phase MARS $\approx$ 0.470, single-phase Volterra $\approx$ 0.482) for Ipswich. The proposed VMD-SA-RF for Gold Coast and Darling Downs regions is also realistically good (Fig. 10).

5. Discussion

The aptness of VMD-SA-RF (benchmarked with the VMD-SA-MARS, VMD-SA-Volterra, single-phase RF, single-phase MARS and single-phase Volterra models) for daily Radn predicting has been explored. The VMD-SA-RF was performed well against the alternative counterpart models in all three study regions, thus clarifying that the VMD-SA-RF was well-designed and better in

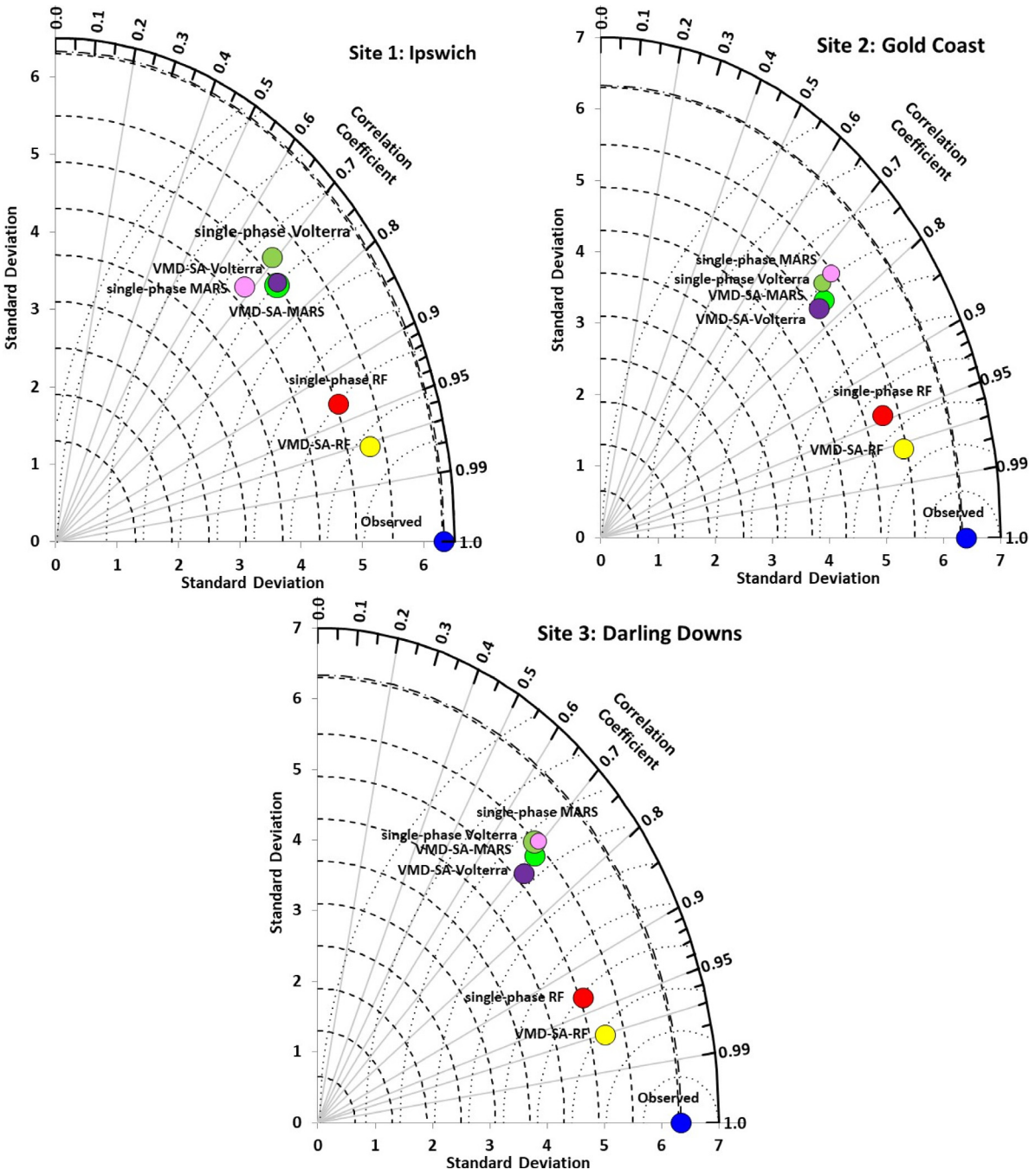

Fig. 6. Taylor diagram depicting the correlation coefficient for the VMD-SA-RF vs. the VMD-SA-MARS, VMD-SA-Volterra, single-phase RF, single-phase MARS and single-phase Volterra models applied at all the three tested stations in Queensland, Australia.

Table 7
Geographic comparison of the accuracy of the VMD-SA-RF vs. VMD-SA-MARS, VMD-SA-Volterra, single-phase RF, single-phase MARS and single-phase Volterra models in terms of (RRMSE, %) and (RMAE, %) computed within the test sites. Note that the best model is boldfaced (**blue**).

	Ipswich		Gold Coast		Darling Downs	
	RRMSE, %	RMAE, %	RRMSE, %	RMAE, %	RRMSE, %	RMAE, %
Single-phase MARS	25.52	25.36	22.68	23.22	25.74	25.01
Single-phase Volterra	25.50	24.75	22.74	23.14	25.93	25.55
Single-phase RF	13.46	13.84	11.67	12.13	13.40	13.87
VMD-SA-MARS	24.36	26.01	21.83	22.21	25.84	25.46
VMD-SA-Volterra	24.13	25.54	21.45	22.14	24.38	25.43
VMD-SA-RF	**9.35**	**9.68**	**8.61**	**8.90**	**9.86**	**10.42**

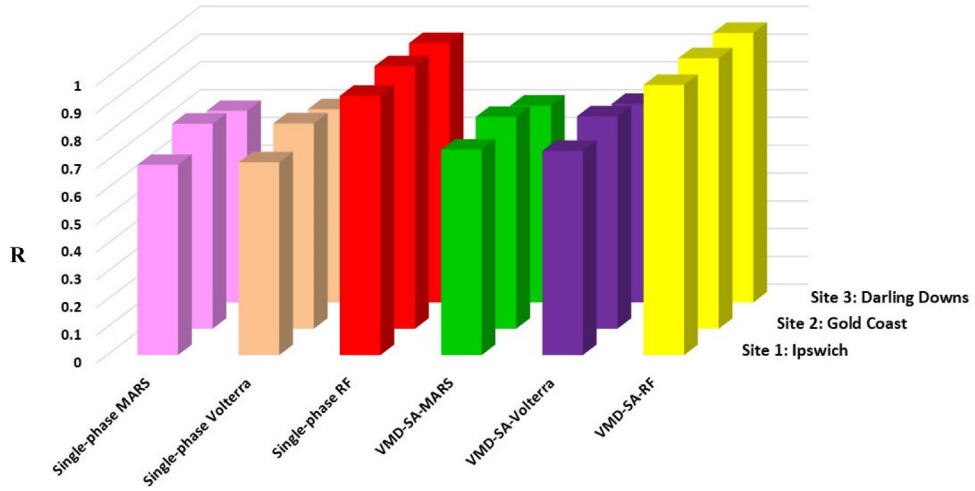

Fig. 7. A comparison of the correlation coefficient for daily Rn forecasting generated by VMD-SA-RF vs. the VMD-SA-MARS, VMD-SA-Volterra, single-phase RF, single-phase MARS and single-phase Volterra models.

mining features from meteorological predictors in an intelligent way. The predicting precision of VMD-SA-RF has discovered that the SA was advantageous in picking the pertinent topographic features to enhance the predicting ability of RF during Radn forecasting.

In accumulation to the overall better performance of VMD-SA-RF, the outcomes also established the suitability and aptness of SA in extracting the pertinent attributes with the statistical metrics for VMD-SA-RF (i.e., Tables 5–7) were extraordinarily better than the counterpart models. Since the data-drive approaches completely influenced by the past historical information which may disturb the 'learning' process, the results here confirm that a suitable feature assortment should be accomplished cautiously in advance to construct these systems. Based on the reported previous studies (Badr and Fahmy, 2004; Cordon et al., 2002; Mullen et al., 2009; Sweetlin et al., 2017), with the monitored approaches is an agreement. Another crucial insight is that fewer input variables require least output relations that result in an intelligent and computationally decent VMD-SA-RF model. Another main achievement is the distinctive input VMD-based signals (i.e., BL-IMFs) arrangements are essential in periodically discovering Radn (Table 2).

Further to hybridization of the RF, MARS and Volterra techniques with SA algorithm, an additional upgrading in model accuracy was obtained by mixing of VMD to decompose the predictors that result into VMD-SA-RF (and VMD-SA-MARS, VMD-SA-Volterra) models. The VMD is effectively categorized and isolate the pertinent attributes from within the meteorological variables to launch a more reliable physical basis for a specific ML technique. In this work the practicality of VMD for several climatic interpreters is engaged for real-time pre-processing data. To obtain simultaneously, the VMD is capable to classify the relevant characteristics of the signal's core frequency.

It is essential to note that the practicability of VMD in forecasting daily Radn is a prominent development in this work, to increase the forecasting skill of the RF, MARS and Volterra models. The performance established that the VMD-SA-RF can deliver healthier and improved predictions of daily Radn for the designated regions in contrast to benchmarking models. It was certainly observed that clear insights of the physical process were provided to the VMD-SA-RF, primarily by the VMD technique, additionally empowering the ML model to successfully handle the information from climatological predictors modelling Radn. One possible aim for improved performance of VMD-SA-RF against standalone counterparts, is feasibly attributable to the additional operational transformation of the data on deterministic processes in weather-related predictors, decomposed into several frequency signals, thus, causing in lower errors and enhanced accuracy.

In addition, a primitive benefit of the VMD as employed in this work is its adaptability and non-recursive behaviour that depends solely on input attributes with trivial human involvement (Dragomiretskiy and Zosso, 2014). Unlike the EMD, the VMD demarcates and updated the input predictors into various IMFs (Looney and Mandic, 2009). The VMD is fundamentally more robust in terms of sampling and noise reduction together with astound accuracy in embedded frequency search and separation. Moreover, the VMD algorithm can aptly extract the time–frequency signals improving the mode mixing issues via band limiting and optimization. Thus, the VMD-SA-RF methodology has the capacity for solar radiation and generation management systems. With historically forecasted Radn, this improved VMD-SA-RF model can agreeably be employed in energy structures to predict future Radn.

For future investigation, the proposed VMD-based hybrid models could be compared to other multi-resolution analysis tools such as the non-decimated maximum-overlap discrete wavelet transformation (MODWT) (Cornish et al., 2006; Percival et al., 2011); the empirical mode decomposition (EMD) (Huang et al., 1998); the ensemble-EMD (EEMD) (Wu and Huang, 2009); the complete ensemble empirical mode decomposition with adaptive noise (CEEMDAN) (Torres et al., 2011); or the improved complete ensemble empirical mode decomposition with adaptive noise (ICEEMDAN) which is the most advanced EMD that is able to address the shortcomings of the predecessor EMD-based algorithms (Colominas et al., 2014). In addition, Radn forecasts at different time-steps should also be investigated in further independent studies. Moreover, other casual related parameters such as ratio between the measured global radiation and the extra-solar radiation or clearness index can be incorporated in the prediction matrix for enhancing the accuracy results.

The established work in the current research is an innovative type and particularly in employing the VMD methodology to decompose climatological variables into their appropriate BL-IMFs signals and then filtered the preeminent candidate features *via* SA and finally predict Radn by implementing RF framework. Enhancing the opportunity and scope of VMD-SA-RF, upcoming studies can implement this model in rainfall, drought, streamflow, flood

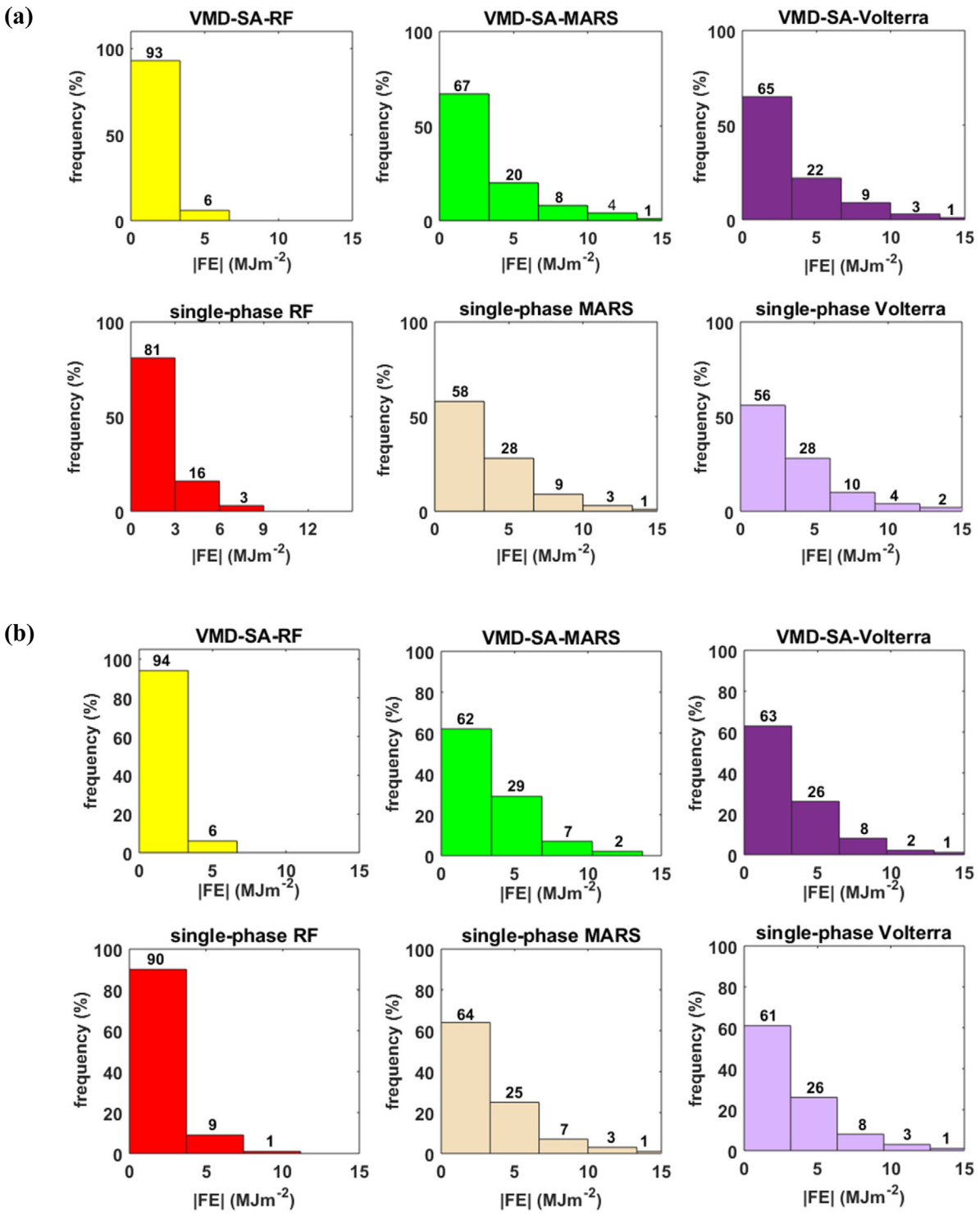

Fig. 8. Frequency plot of the absolute forecasted error, |FE| generated by VMD-SA-RF vs. the VMD-SA-MARS, VMD-SA-Volterra, single-phase RF, single-phase MARS and single-phase Volterra models in the test phase.

events and energy demand, to allow agencies and institutions to manage the climate change calamities.

6. Conclusions

A substantial contribution towards Radn prediction scenarios was made by constructing a robust ML model combining best and apt predictors features extracted from a set of VMD based BL-IMFs operating the SA approach. The demarcated input datasets were centred on the historical lags of the weather-related inputs in the model's training process to predict the Radn for three rich solar regions in Australia. Near-real-time daily datasets over the period January 1905–23 June 2018 were demarcated into their analogous BL-IMFs signals *via* VMD where the SA was hired to screen out the best BL-IMFs. The selected BL-IMFs were incorporated into the RF to build the VMD-SA-RF model, and the succeeding model's accuracy was gauged by VMD-SA-MARS, VMD-SA-Volterra and single-phase RF, single-phase MARS and

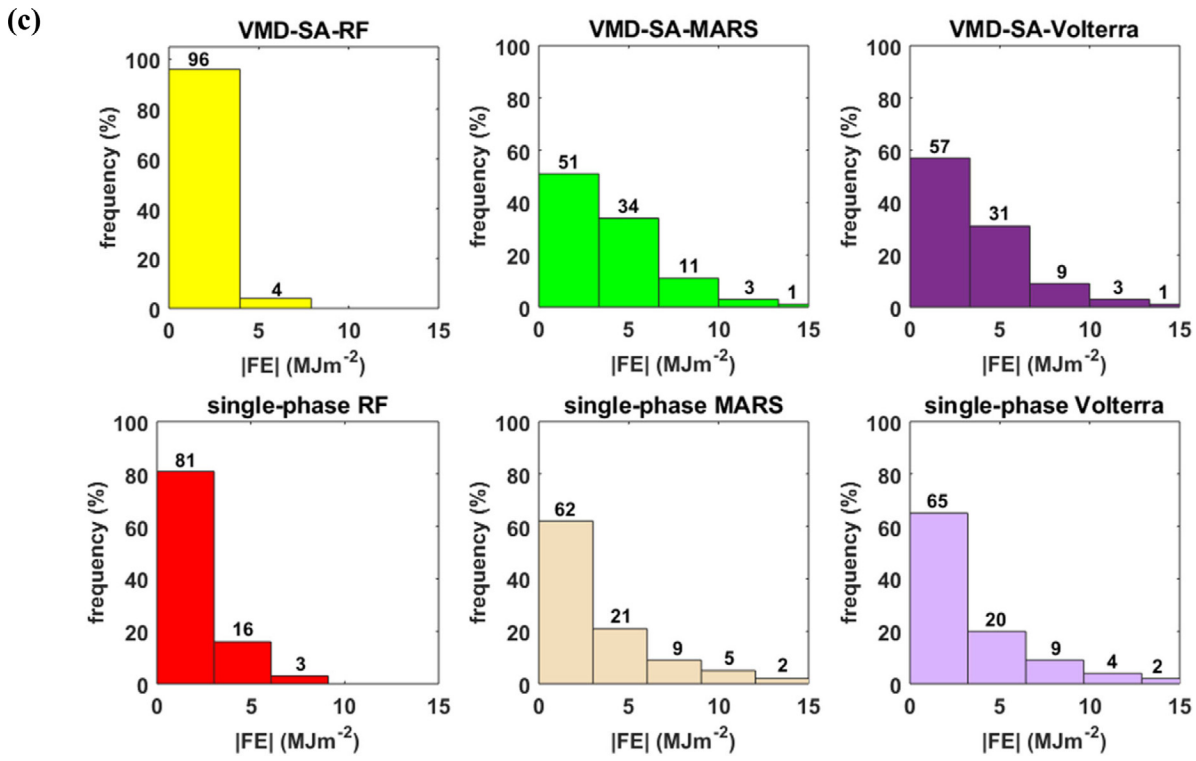

Fig. 8. (*continued*).

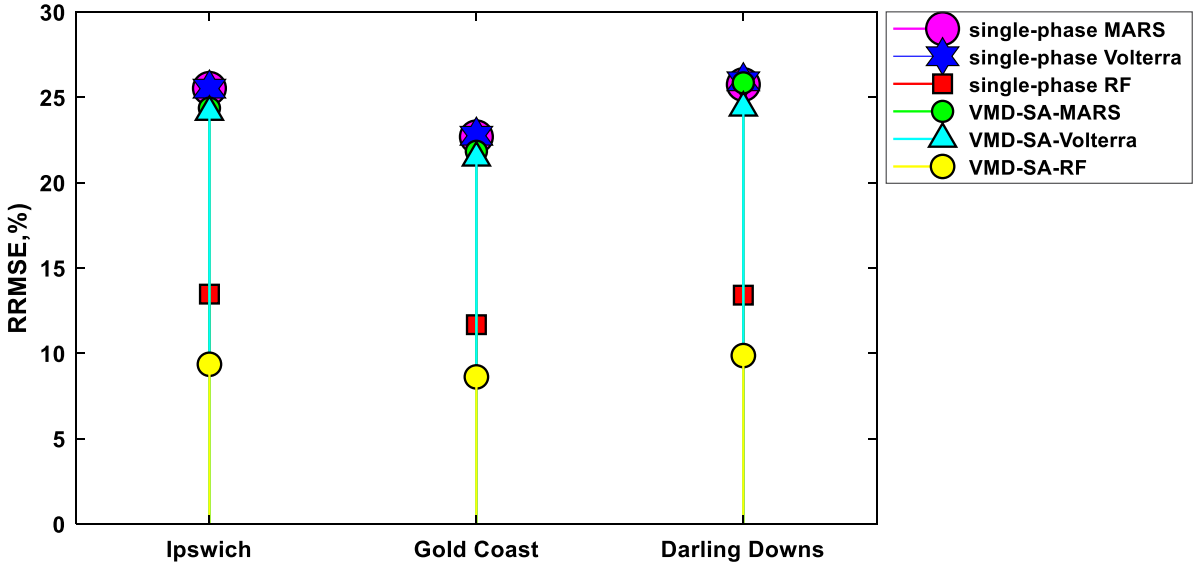

Fig. 9. Stem plot of the relative mean absolute error (RMSE, %) generated by VMD-SA-RF vs. the VMD-SA-MARS, VMD-SA-Volterra, single-phase RF, single-phase MARS and single-phase Volterra models.

single-phase Volterra RF models. The statistical results indicated that the RRMSPE and RMAPE errors were found approximately 8.61%, 8.90% for VMD-SA-RF compared with 21.83%, 22.21% for VMD-SA-MARS, 21.45%, 22.14% for VMD-SA-Volterra models, that contrasted a value of 11.67%, 12.13% for single-phase RF, 22.68%, 23.22% for single-phase MARS and 22.74%, 23.14% for single-phase Volterra model in the case Gold Coast to predict Radn. A significant number of geographical variations in the model performances were also apparent for the VMD-SA-RF via RRMSPE and RMAPE, where an optimal precision was achieved for Gold Coast against Ipswich and Darling Downs. To conclude, the solar radiation forecasting framework designed in this research work can also agreeably allow politicians and Govt representatives in renewable and sustainable energy generation comprising decisions on infrastructural areas and, better the practical applications (e.g., smart grids, solar PV generation reliability) and other scenarios in the present era of climate variability to utilize ML models for intelligent and informed decisions.

Abbreviations

band-limited intrinsic mode functions (BL-IMFs), basis functions (BF), Cascade Forecasting Architecture (CFA), Coefficient of Correlation (R), complete ensemble EMD with adaptive noise

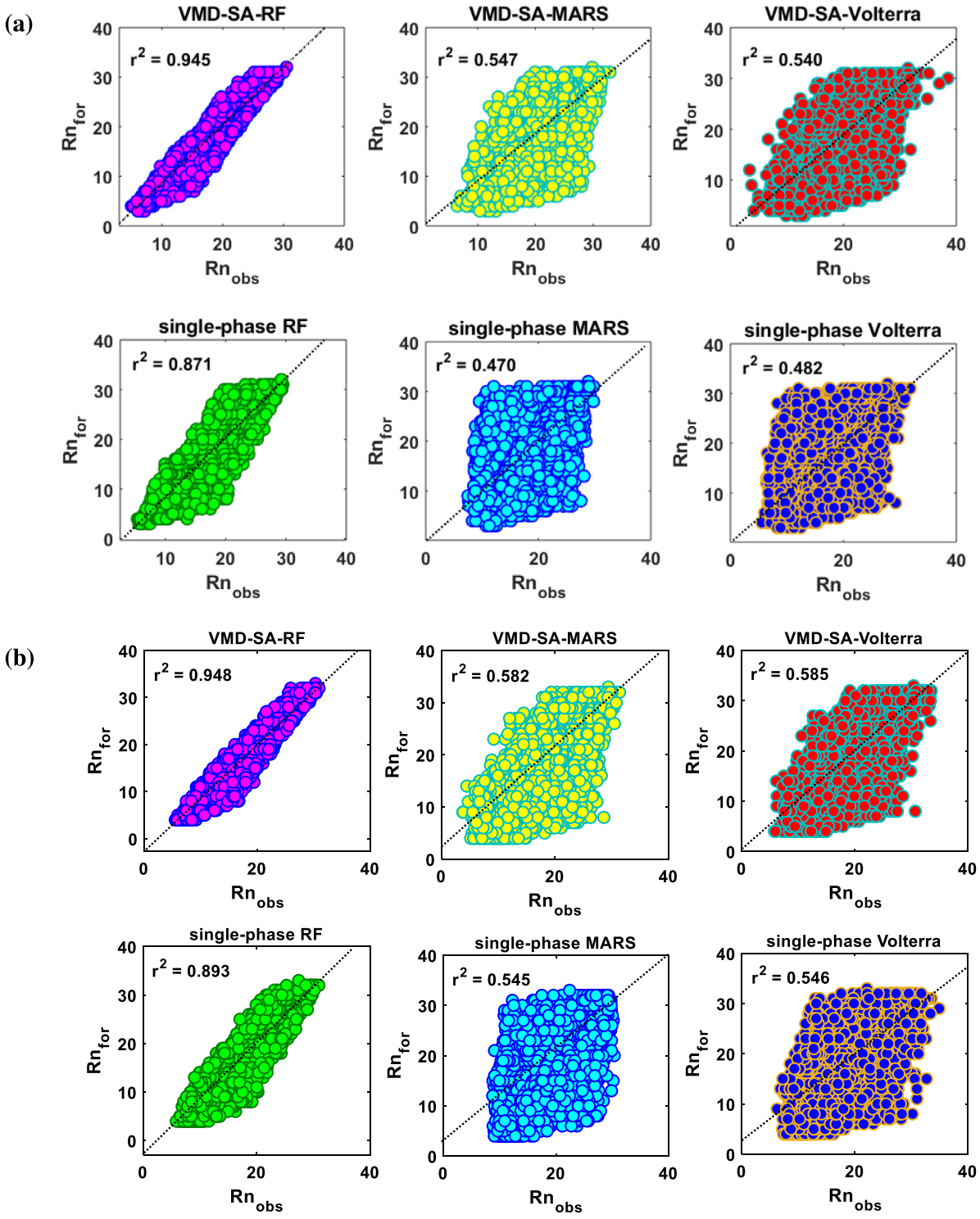

Fig. 10. Scatterplots of forecasted vs. observed daily solar radiation Rn for the tested sites in Australia. A least square regression line and coefficient of determination (r^2) with a linear fit equation inserted in each sub-panel.

(CEEMDAN), Empirical Mode Decomposition (EMD), discrete wavelet transformation (DWT), evaporation (Evap), ensemble-EMD (EEMD), Gaussian process regression (GPR), Generalized Cross Validation (GCV), improved complete ensemble empirical mode decomposition with adaptive noise (ICEEMDAN), Legates and McCabe's (E_{LM}), machine learning (ML), maximum-overlap discrete wavelet transformation (MODWT), Mean absolute error (MAE), maximum temperature ($T_{max,}$), minimum temperature (T_{min}), monthly precipitation (Rain), multi-resolution analysis (MRA), Multivariate adaptive regression splines (MARS), Nash–Sutcliffe efficiency (E_{NS}), Parallel Forecasting Architecture (PFA), Random Forest (RF), Root mean square error (RMSE), Relative Humidity at maximum temperature (RH_{max}.T), Relative Humidity

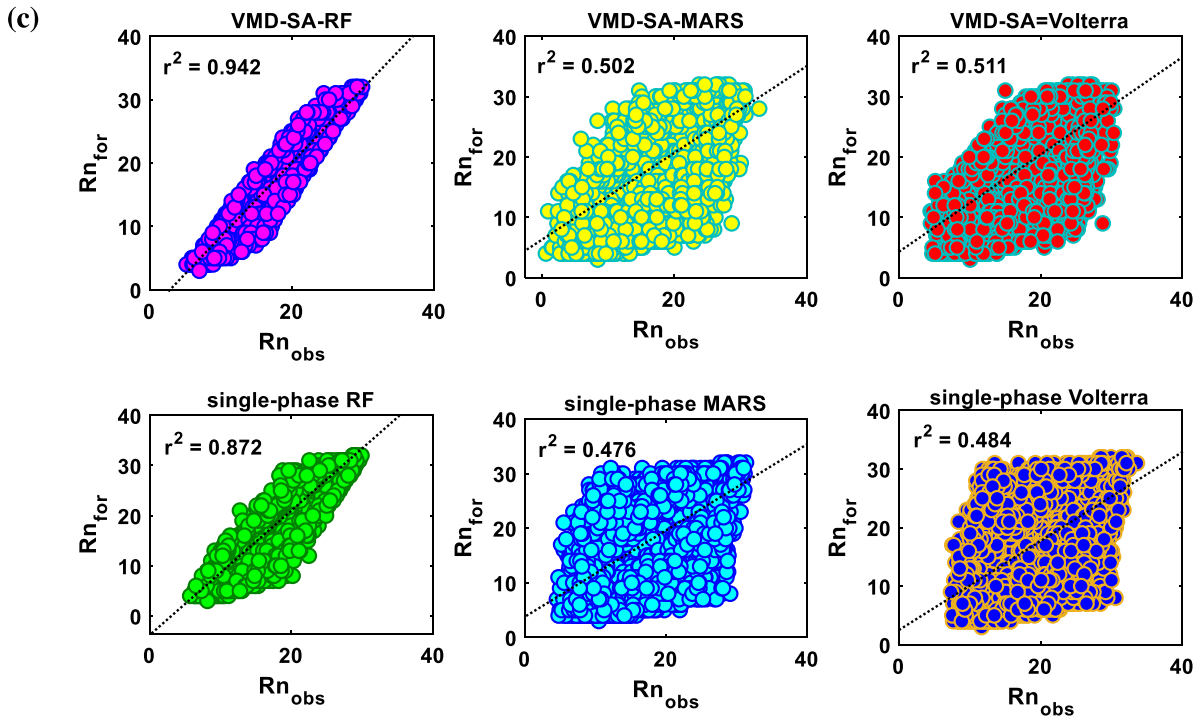

Fig. 10. (*continued*).

at minimum temperature (RH_{min}.T), Relative mean absolute percentage error (RMAPE; %), Relative root mean squared percentage error (RRMSPE; %), Scientific Information for Land Owners (SILO), simulated annealing (SA), solar photovoltaic (PV), small-scale renewable energy schemes (SRES), solar radiation (Radn), variational mode decomposition (VMD), vapour pressure (VP), weighted Gaussian process regression (WGPR), Willmott's Index (E_{WI}).

CRediT authorship contribution statement

Mumtaz Ali: Conceptualization, Methodology, Modelling, Manuscript writing. **Ramendra Prasad:** Validation, Investigation, Data organization, Manuscript writing. **Yong Xiang:** Supervision, Manuscript editing, Manuscript writing, Validation. **Mohsin Khan:** Results analysis and discussion, Manuscript writing, Investigation, Methodology. **Aitazaz Ahsan Farooque:** Conceptualization, Validation, Investigation, Supervision, Manuscript writing. **Tianrui Zong:** Manuscript revision and editing, Manuscript writing, Validation, Analysis. **Zaher Mundher Yaseen:** Project leader, Conceptualization, Validation, Investigation, Analysis, Manuscript writing.

Declaration of competing interest

The authors declare that they have no known competing financial interests or personal relationships that could have appeared to influence the work reported in this paper.

Acknowledgement

The authors are thankful to Scientific Information for Landowners (SILO) to provide the relevant meteorological and solar radiation data. The authors state that there is no conflict of interest.

References

Abbas, E.F., Azat, S.A., 2018. The impact of width of the air gap channel on the mass flow rate, Rayleigh number, and efficiency of passive solar heating system. Tikrit J. Eng. Sci. 25, 47–52.

Al-Sulttani, A.O., Al-Mukhtar, M., Roomi, A.B., Farooque, A., Khedher, K.M., Yaseen, Z.M., 2021. Proposition of new ensemble data-intelligence models for surface water quality prediction. IEEE Access.

Ali, M., Deo, R.C., Maraseni, T., Downs, N.J., 2019. Improving SPI-derived drought forecasts incorporating synoptic-scale climate indices in multi-phase multivariate empirical mode decomposition model hybridized with simulated annealing and kernel ridge regression algorithms. J. Hydrol. http://dx.doi.org/10.1016/j.jhydrol.2019.06.032.

Ali, M., Prasad, R., 2019. Significant wave height forecasting via an extreme learning machine model integrated with improved complete ensemble empirical mode decomposition. Renew. Sustain. Energy Rev. http://dx.doi.org/10.1016/j.rser.2019.01.014.

Ali, M., Prasad, R., Xiang, Y., Yaseen, Z.M., 2020. Complete ensemble empirical mode decomposition hybridized with random forest and kernel ridge regression model for monthly rainfall forecasts. J. Hydrol. http://dx.doi.org/10.1016/j.jhydrol.2020.124647.

Alvanitopoulos, P.-F., Andreadis, I., Georgoulas, N., Zervakis, M., Nikolaidis, N., 2014. Solar radiation time-series prediction based on empirical mode decomposition and artificial neural networks. Prog. Pattern recognition. Image Anal. Comput. Vis. Appl. http://dx.doi.org/10.1007/978-3-662-44654-6_44.

Athier, G., Floquet, P., Pibouleau, L., Domenech, S., 1997. Synthesis of heat-exchanger network by simulated annealing and NLP procedures. AIChE J. 43, 3007–3020. http://dx.doi.org/10.1002/aic.690431113.

Badr, A., Fahmy, A., 2004. A proof of convergence for ant algorithms. Inf. Sci. (NY) 160, 267–279.

Beesley, C., Frost, A., Zajaczkowski, J., 2009. A comparison of the BAWAP and SILO spatially interpolated daily rainfall datasets. In: 18th World IMACS/MODSIM Congress. Citeseer, Cairns, Australia, pp. 13–17.

Bhagat, S.K., Tiyasha, T., Tung, T.M., Mostafa, R.R., Yaseen, Z.M., 2020. Manganese (Mn) removal prediction using extreme gradient model. Ecotoxicol. Environ. Saf. 204, 111059. http://dx.doi.org/10.1016/j.ecoenv.2020.111059.

Breiman, L., 1996. Bagging predictors. Mach. Learn. 24, 123–140. http://dx.doi.org/10.1007/BF00058655.

Breiman, L., 2001. Random forests. Mach. Learn. 45, 5–32. http://dx.doi.org/10.1023/A:1010933404324.

Chester, L., Elliot, A., Crossley, P., 2018. New forms of solar PV provisioning needed to advance energy justice for lower income households. In: Asia Pacific Solar Research Conference. 4–6 December 2018, Sydney, Australia.

Colominas, M.A., Schlotthauer, G., Torres, M.E., 2014. Improved complete ensemble EMD: A suitable tool for biomedical signal processing. Biomed. Signal Process. Control 14, 19–29. http://dx.doi.org/10.1016/j.bspc.2014.06.009.

Cordon, O., Herrera, F., Stützle, T., 2002. A review on the ant colony optimization metaheuristic: Basis, models and new trends. Mathw. Comput.
Cornish, C.R., Bretherton, C.S., Percival, D.B., 2006. Maximal overlap wavelet statistical analysis with application to atmospheric turbulence. Bound.-Layer Meteorol. 119, 339–374. http://dx.doi.org/10.1007/s10546-005-9011-y.
Dowsland, K.A., Thompson, J., 2012. Simulated annealing. Handb. Nat. Comput 1623–1655.
Dragomiretskiy, K., Zosso, D., 2014. Variational mode decomposition. IEEE Trans. Signal Process. 62, 531–544. http://dx.doi.org/10.1109/tsp.2013.2288675.
Du, H., Fan, J., He, X., Feldman, M.W., 2018. A genetic simulated annealing algorithm to optimize the small-world network generating process. Complexity http://dx.doi.org/10.1155/2018/1453898.
Elleithy, K.M., Fattah, E.G., 2012. A Simulated Annealing Algorithm for Register Allocation. Citeseer.
Friedman, J.H., 1991. Multivariate adaptive regression splines. Ann. Statist. 19, 1–67. http://dx.doi.org/10.1214/aos/1176347963.
Guermoui, M., Gairaa, K., Rabehi, A., Djafer, D., Benkaciali, S., 2018a. Estimation of the daily global solar radiation based on the Gaussian process regression methodology in the Saharan climate. Eur. Phys. J. Plus 133, http://dx.doi.org/10.1140/epjp/i2018-12029-7.
Guermoui, M., Melgani, F., Danilo, C., 2018b. Multi-step ahead forecasting of daily global and direct solar radiation: A review and case study of ghardaia region. J. Clean. Prod. http://dx.doi.org/10.1016/j.jclepro.2018.08.006.
Guermoui, M., Melgani, F., Gairaa, K., Mekhalfi, M.L., 2020. A comprehensive review of hybrid models for solar radiation forecasting. J. Clean. Prod. 258, 120357. http://dx.doi.org/10.1016/j.jclepro.2020.120357.
Hai, T., Sharafati, A., Mohammed, A., Salih, S.Q., Deo, R.C., Al-Ansari, N., Yaseen, Z.M., 2020. Global solar radiation estimation and climatic variability analysis using extreme learning machine based predictive model. IEEE Access 8, 12026–12042. http://dx.doi.org/10.1109/access.2020.2965303.
Hou, M., Zhang, T., Weng, F., Ali, M., Al-Ansari, N., Yaseen, Z., 2018. Global solar radiation prediction using hybrid online sequential extreme learning machine model. Energies 11, 3415.
Hsu, C.-W., Chang, C.-C., Lin, C.-J., 2003. A practical guide to support vector classification. BJU Int. http://dx.doi.org/10.1177/02632760022050997.
Huang, N.E., Shen, Z., Long, S.R., Wu, M.C., Snin, H.H., Zheng, Q., Yen, N.C., Tung, C.C., Liu, H.H., 1998. The empirical mode decomposition and the Hubert spectrum for nonlinear and non-stationary time series analysis. Proc. R. Soc. A Math. Phys. Eng. Sci. http://dx.doi.org/10.1098/rspa.1998.0193.
Jeffrey, S.J., Carter, J.O., Moodie, K.B., Beswick, A.R., 2001. Using spatial interpolation to construct a comprehensive archive of Australian climate data. Environ. Model. Softw. 16, 309–330. http://dx.doi.org/10.1016/s1364-8152(01)00008-1.
Khelifi, R., Guermoui, M., Rabehi, A., Lalmi, D., 2020. Multi-step-ahead forecasting of daily solar radiation components in the Saharan climate. Int. J. Ambient Energy 41, 707–715.
Kirkpatrick, S., Gelatt, C.D., Vecchi, M.P., 1983. Optimization by simulated annealing. Science 80, http://dx.doi.org/10.1126/science.220.4598.671.
Labat, D., Ababou, R., Mangin, A., 2001. Introduction of wavelet analyses to rainfall/runoffs relationship for a Karstic Basin: The case of Licq-Atherey Karstic System (France). Ground Water 39, 605–615. http://dx.doi.org/10.1111/j.1745-6584.2001.tb02348.x.
Li, Z., Chen, J., Zi, Y., Pan, J., 2017. Independence-oriented VMD to identify fault feature for wheel set bearing fault diagnosis of high speed locomotive. Mech. Syst. Signal Process 85, 512–529. http://dx.doi.org/10.1016/j.ymssp.2016.08.042.
Looney, D., Mandic, D.P., 2009. Multiscale image fusion using complex extensions of EMD. IEEE Trans. Signal Process. http://dx.doi.org/10.1109/TSP.2008.2011836.
Maheswaran, R., Khosa, R., 2012a. Comparative study of different wavelets for hydrologic forecasting. Comput. Geosci. 46, 284–295. http://dx.doi.org/10.1016/j.cageo.2011.12.015.
Maheswaran, R., Khosa, R., 2012b. Wavelet-Volterra coupled model for monthly stream flow forecasting. J. Hydrol. 450–451, 320–335. http://dx.doi.org/10.1016/j.jhydrol.2012.04.017.
Mahmmoud, O.N., Gaeid, K.S., Nashi, A.F., Siddiqui, K.M., 2020. Induction motor speed control with solar cell using MPPT algorithm by incremental conductance method. Tikrit J. Eng. Sci. 27, 8–16.
Majumder, I., Dash, P.K., Bisoi, R., 2018. Variational mode decomposition based low rank robust kernel extreme learning machine for solar irradiation forecasting. Energy Convers. Manag. 171, 787–806. http://dx.doi.org/10.1016/j.enconman.2018.06.021.
Mohammed, B.F., 2018. Position control of solar panel receiver by joint generated power and received signal power maximization. Tikrit J. Eng. Sci. 25.
Mohmmoud, O.N., 2020. Design and implement of dual axis solar tracker system based arduino. Tikrit J. Eng. Sci. 27, 71–81.
Mullen, R.J., Monekosso, D., Barman, S., Remagnino, P., 2009. A review of ant algorithms. Expert Syst. Appl. http://dx.doi.org/10.1016/j.eswa.2009.01.020.
Peng, M., Gupta, N.K., Armitage, A.F., 1996. An investigation into the improvement of local minima of the hopfield network. Neural Net. 9, 1241–1253. http://dx.doi.org/10.1016/0893-6080(96)00017-2.
Percival, D.B., Lennox, S.M., Wang, Y.-G., Darnell, R.E., 2011. Wavelet-based multiresolution analysis of Wivenhoe Dam water temperatures. Water Resour. Res. 47, http://dx.doi.org/10.1029/2010wr009657.
Prasad, R., Deo, R.C., Li, Y., Maraseni, T., 2018. Soil moisture forecasting by a hybrid machine learning technique: ELM integrated with ensemble empirical mode decomposition. Geoderma 330, 136–161. http://dx.doi.org/10.1016/j.geoderma.2018.05.035.
Prasad, R., Deo, R.C., Li, Y., Maraseni, T., 2019. Weekly soil moisture forecasting with multivariate sequential, ensemble empirical mode decomposition and Boruta-random forest hybridizer algorithm approach. CATENA 177, 149–166. http://dx.doi.org/10.1016/j.catena.2019.02.012.
Rathinasamy, M., Khosa, R., Adamowski, J., ch, S., Partheepan, G., Anand, J., Narsimlu, B., 2014. Wavelet-based multiscale performance analysis: An approach to assess and improve hydrological models. Water Resour. Res. 50, 9721–9737. http://dx.doi.org/10.1002/2013wr014650.
Salih, S.Q., sharafati, A., Khosravi, K., Faris, H., Kisi, O., Tao, H., Ali, M., Yaseen, Z.M., 2019. River suspended sediment load prediction based on river discharge information: application of newly developed data mining models. Hydrol. Sci. J. 1–14. http://dx.doi.org/10.1080/02626667.2019.1703186.
Sangrody, H., Sarailoo, M., Zhou, N., Tran, N., Motalleb, M., Foruzan, E., 2017. Weather forecasting error in solar energy forecasting. IET Renew. Power Gener. 11, 1274–1280. http://dx.doi.org/10.1049/iet-rpg.2016.1043.
Shamseldin, A.Y., 1997. Application of a neural network technique to rainfall-runoff modelling. J. Hydrol. http://dx.doi.org/10.1016/S0022-1694(96)03330-6.
Sharafati, A., Khosravi, K., Khosravinia, P., Ahmed, K., Salman, S.A., Mundher, Z., Shamsuddin, Y., 2019. The potential of novel data mining models for global solar radiation prediction. Int. J. Environ. Sci. Technol. http://dx.doi.org/10.1007/s13762-019-02344-0.
Soman, K.P., Poornachandran, P., Athira, S., Harikumar, K., 2015. Recursive variational mode decomposition algorithm for real time power signal decomposition. Procedia Technol. 21, 540–546.
Stock, P., Bourne, G., Hussey, K., 2017. Renewables: powering Queensland's future.
Sweetlin, J.D., Nehemiah, H.K., Kannan, A., 2017. Feature selection using ant colony optimization with tandem-run recruitment to diagnose bronchitis from CT scan images. Comput. Methods Programs Biomed. http://dx.doi.org/10.1016/j.cmpb.2017.04.009.
Taniguchi, M., Kurokawa, K., Itoh, K., Matsuoka, K., Ichioka, Y., 1997. Sidelobeless multiple-object discriminant filters recorded as discrete-type computer-generated holograms. Appl. Opt. 36, 9138. http://dx.doi.org/10.1364/ao.36.009138.
Tiyasha, T., Tung, T.M., Bhagat, S.K., Tan, M.L., Jawad, A.H., Mohtar, W.H.M.W, Yaseen, Z.M., 2021. Functionalization of remote sensing and on-site data for simulating surface water dissolved oxygen: Development of hybrid tree-based artificial intelligence models. Mar. Pollut. Bull. 170, 112639.
Tiyasha, T.M., Yaseen, Z.M., 2020. A survey on river water quality modelling using artificial intelligence models: 2000–2020. J. Hydrol. http://dx.doi.org/10.1016/j.jhydrol.2020.124670.
Torres, M.E., Colominas, M.A., Schlotthauer, G., Flandrin, P., 2011. A complete ensemble empirical mode decomposition with adaptive noise. In: 2011 IEEE Int. Conf. Acoust. Speech Signal Process. http://dx.doi.org/10.1109/icassp.2011.5947265.
Tur, R., Yontem, S., 2021. A comparison of soft computing methods for the prediction of wave height parameters. Knowl.-Based Eng. Sci. 2, 31–46.
Wang, D., Liu, Y., Luo, H., Yue, C., Cheng, S., 2017. Day-ahead PM2.5 concentration forecasting using WT-VMD based decomposition method and back propagation neural network improved by differential evolution. Int. J. Environ. Res. Public Health 14, 764. http://dx.doi.org/10.3390/ijerph14070764.
Wilson, J.D., 1997. A simulated annealing algorithm for optimizing RF power efficiency in coupled-cavity traveling-wave tubes. IEEE Trans. Electron Devices 44, 2295–2299. http://dx.doi.org/10.1109/16.644656.
Wu, Z., Huang, N., 2009. Ensemble empirical mode decomposition: A noise-assisted data analysis method. Adv. Adapt. Data Anal. 01, 1–41. http://dx.doi.org/10.1142/s1793536909000047.
Wu, Z., Huang, N.E., Wallace, J.M., Smoliak, B.V., Chen, X., 2011. On the time-varying trend in global-mean surface temperature. Clim. Dyn. 37, 759–773. http://dx.doi.org/10.1007/s00382-011-1128-8.
Yang, X.-S., 2020. Nature-inspired optimization algorithms: Challenges and open problems. J. Comput. Sci 46, 101104.
Yaseen, Z.M., 2021. An insight into machine learning models era in simulating soil, water bodies and adsorption heavy metals: Review, challenges and solutions. Chemosphere 130126.
Zahedi, A., 2010. Australian renewable energy progress. Renew. Sustain. Energy Rev. 14, 2208–2213. http://dx.doi.org/10.1016/j.rser.2010.03.026.
Zajaczkowski, J., Wong, K., Carter, J., 2013. Improved historical solar radiation gridded data for Australia. Environ. Model. Softw. 49, 64–77. http://dx.doi.org/10.1016/j.envsoft.2013.06.013.
Zhang, G., Liu, H., Zhang, J., Yan, Y., Zhang, L., Wu, C., Hua, X., Wang, Y., 2018. Wind power prediction based on variational mode decomposition multi-frequency combinations. J. Mod. Power Syst. Clean Energy 7, 281–288. http://dx.doi.org/10.1007/s40565-018-0471-8.
Zhou, J., Sun, N., Jia, B., Peng, T., 2018. A novel decomposition-optimization model for short-term wind speed forecasting. Energies 11, 1752. http://dx.doi.org/10.3390/en11071752.